Article

Terminal Gold-Oxo Complexes

Rui Cao, Travis M. Anderson, Paula M. B. Piccoli, Arthur J. Schultz, Thomas F. Koetzle, Yurii V. Geletii, Elena Slonkina, Britt Hedman, Keith O. Hodgson, Kenneth I. Hardcastle, Xikui Fang, Martin L. Kirk, Sushilla Knottenbelt, Paul Kgerler, Djamaladdin G. Musaev, Keiji Morokuma, Masashi Takahashi, and Craig L. Hill

J. Am. Chem. Soc., **2007**, 129 (36), 11118-11133• DOI: 10.1021/ja072456n • Publication Date (Web): 21 August 2007

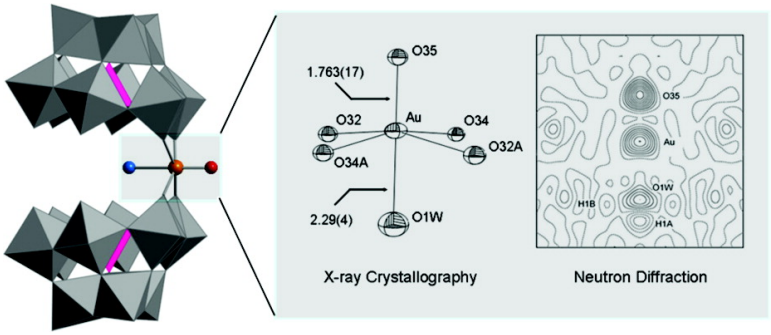

More About This Article

Additional resources and features associated with this article are available within the HTML version:

- Supporting Information
- Links to the 11 articles that cite this article, as of the time of this article download
- Access to high resolution figures
- Links to articles and content related to this article
- Copyright permission to reproduce figures and/or text from this article

View the Full Text HTML

J|A|C|S
ARTICLES
Published on Web 08/21/2007

Terminal Gold-Oxo Complexes

Rui Cao,[†] Travis M. Anderson,[†] Paula M. B. Piccoli,[‡] Arthur J. Schultz,[‡] Thomas F. Koetzle,[‡] Yurii V. Geletii,[†] Elena Slonkina,[§] Britt Hedman,[§] Keith O. Hodgson,[§] Kenneth I. Hardcastle,[†] Xikui Fang,[†] Martin L. Kirk,[∥] Sushilla Knottenbelt,[∥] Paul Kögerler,[⊥] Djamaladdin G. Musaev,[#] Keiji Morokuma,[†,#] Masashi Takahashi,[@] and Craig L. Hill*[,†]

Contribution from the Department of Chemistry, Emory University, Atlanta, Georgia 30322, Intense Pulsed Neutron Source, Argonne National Laboratory, Argonne, Illinois 60439, Department of Chemistry and Stanford Synchrotron Radiation Laboratory, Stanford University, Stanford, California 94305, Department of Chemistry and Chemical Biology, The University of New Mexico, Albuquerque, New Mexico 87131−0001, Ames Laboratory, Iowa State University, Ames, Iowa 50011, Cherry L. Emerson Center for Scientific Computation, Emory University, Atlanta, Georgia 30322, and Department of Chemistry, Faculty of Science, Toho University, Miyama, Funabashi, Chiba 274-8510, Japan

Received April 8, 2007; E-mail: chill@emory.edu

Abstract: In contradiction to current bonding paradigms, two terminal Au-oxo molecular complexes have been synthesized by reaction of $AuCl_3$ with metal oxide-cluster ligands that model redox-active metal oxide surfaces. Use of $K_{10}[\alpha_2\text{-}P_2W_{17}O_{61}]\cdot 20H_2O$ and K_2WO_4 (forming the $[A\text{-}PW_9O_{34}]^{9-}$ ligand *in situ*) produces $K_{15}H_2[Au(O)(OH_2)P_2W_{18}O_{68}]\cdot 25H_2O$ (**1**); use of $K_{10}[P_2W_{20}O_{70}(OH_2)_2]\cdot 22H_2O$ (**3**) produces $K_7H_2[Au(O)(OH_2)\text{-}P_2W_{20}O_{70}(OH_2)_2]\cdot 27H_2O$ (**2**). Complex **1** crystallizes in orthorhombic *Fddd*, with $a = 28.594(4)$ Å, $b = 31.866(4)$ Å, $c = 38.241(5)$ Å, $V = 34844(7)$ Å^3, $Z = 16$ (final $R = 0.0540$), and complex **2** crystallizes in hexagonal *P*6(3)/*mmc*, with $a = 16.1730(9)$ Å, $b = 16.1730(9)$ Å, $c = 19.7659(15)$ Å, $V = 4477.4(5)$ Å^3, $Z = 2$ (final $R = 0.0634$). The polyanion unit in **1** is disorder-free. Very short (∼1.76 Å) Au-oxo distances are established by both X-ray and 30 K neutron diffraction studies, and the latter confirms oxo and *trans* aqua (H_2O) ligands on Au. Seven findings clarify that Au and not W is present in the Au-oxo position in **1** and **2**. Five lines of evidence are consistent with the presence of d^8 Au(III) centers that are stabilized by the flanking polytungstate ligands in both **1** and **2**: redox titrations, electrochemical measurements, 17 K optical spectra, Au L_2 edge X-ray absorption spectroscopy, and Au-oxo bond distances. Variable-temperature magnetic susceptibility data for crystalline **1** and **2** establish that both solids are diamagnetic, and ^{31}P and ^{17}O NMR spectroscopy confirm that both remain diamagnetic in solution. Both complexes have been further characterized by FT-IR, thermogravimetric analysis (TGA), differential scanning calorimetry (DSC), and other techniques.

Introduction

Inorganic, organometallic, and catalytic chemists and chemical engineers have speculated whether terminal metal-oxo (O^{2-}) complexes of the late-transition-metal elements may exist as transient intermediates in systems ranging from Cu oxidase enzymes to the surfaces of noble metal oxidation catalysts.[1−10] Despite decades of speculation and attempted synthesis, no terminal metal-oxo complexes of any element to the right of Ru in the periodic table had been reported prior to 2004 with the exception of the d^4 $(mesityl)_3Ir^V$-oxo complex of G. Wilkinson and co-workers,[11] a complex shown subsequently by S. Brown and co-workers to catalyze oxo transfer to phosphines.[12] Terminal metal-oxo complexes of the workhorse catalytic elements in industry, Pd, Au, and in particular Pt, have remained elusive. Given the importance of these elements in O_2-based technologies ranging from catalytic converters (Pt,

[†] Department of Chemistry, Emory University.
[‡] Argonne National Laboratory.
[§] Stanford University.
[∥] The University of New Mexico.
[⊥] Iowa State University.
[#] Cherry L. Emerson Center for Scientific Computation, Emory University.
[@] Toho University.

(1) Nugent, W. A.; Mayer, J. M. *Metal-Ligand Multiple Bonds*; John Wiley & Sons, Inc.: New York, 1988.
(2) Holm, R. H. *Chem. Rev.* **1987**, *87*, 1401−1449.
(3) Morris, R. J.; Girolami, G. S. *Polyhedron* **1988**, *7*, 2001−2008.
(4) Spaltenstein, E.; Erikson, T. K. G.; Critchlow, S. C.; Mayer, J. M. *J. Am. Chem. Soc.* **1989**, *111*, 617−623.
(5) Holm, R. H.; Donahue, J. P. *Polyhedron* **1993**, *12*, 571−589.
(6) Parkin, G. In *Progress in Inorganic Chemistry*; Karlin, K. D., Ed.; Wiley: New York, 1998; Vol. 47, pp 1−165.
(7) MacBeth, C. E.; Golombek, A. P.; Young, Jr., V. G.; Yang, C.; Kuczera, K.; Hendrich, M. P.; Borovik, A. S. *Science* **2000**, *289*, 938−941.
(8) Rohde, J.-U.; In, J.-H.; Lim, M. H.; Brennessel, W. W.; Bukowski, M. R.; Stubna, A.; Münck, E.; Nam, W.; Que, Jr., L. *Science* **2003**, *299*, 1037−1039.
(9) Green, M. T.; Dawson, J. H.; Gray, H. B. *Science* **2004**, *304*, 1653−1656.
(10) Visser, S. P. d.; Kumar, D.; Neumann, R.; Shaik, S. *Angew. Chem., Int. Ed.* **2004**, *43*, 5661−5665.
(11) Hay-Motherwell, R. S.; Wilkinson, G.; Hussain-Bates, B.; Hursthouse, M. B. *Polyhedron* **1993**, *12*, 2009−2012.
(12) Jacobi, B. G.; Laitar, D. S.; Pu, L.; Wargocki, M. F.; DiPasquale, A. G.; Fortner, K. C.; Schuck, S. M.; Brown, S. N. *Inorg. Chem.* **2002**, *41*, 4815−4823.

 10.1021/ja072456n CCC: $37.00

Pd),[13] fuel cell cathodes (Pt, others),[14−18] and catalysts for low-temperature green O_2-based oxidations (Au, Pt, Pd, Ag, etc.),[19−37] the inability of the investigators to realize any terminal metal-oxo species of these elements is noteworthy. The considerable recent research on metal-oxo systems in biology, chemistry, and materials science has been mirrored by noteworthy developments involving mid- and late-transition-metal complexes with terminal multiply bonded ligands in general.[38−67]

The bonds of Pt, Au, and other noble-metal elements to oxygen, while weak, were well established from classical diffraction studies of the metal oxides years ago.[68,69] More recently, well characterized compounds with bridging oxygens bound to both Pt or Au, largely the work of Sharp[70,71] and Cinellu,[72−75] respectively, have been reported. Au−O bonds, including those in the Au_2O_2 unit, which might be viewed as a dimer of terminal Au-oxo units, have recently been characterized in several molecules.[73] However, all known Au−O bonds are long (1.90 to 2.10 Å), consistent with a weaker Au−O interaction. In contrast to bridging or longer and weaker metal−oxygen units, terminal or multiply bonded metal−oxygen units of these elements necessitate significant population of orbitals that are antibonding in the M−O unit, rendering these units unstable.

In late 2004 we reported that use of appropriate polytungstates[76−82] which share structural and reactivity features in common with the metal oxides of broad importance in catalytic technologies (TiO_2, CeO_2, etc.) can facilitate stabilization and isolation of a terminal Pt-oxo complex, $K_7Na_9[Pt^{IV}(O)(OH_2)$-

(13) Shelef, M. *Chem. Rev.* **1995**, *95*, 209−225.
(14) Appleby, A. J.; Foulkes, F. R. *Fuel Cell Handbook*; Krieger Publishing Company, Malabar, FL, 1993.
(15) Somorjai, G. A. *Introduction to Surface Chemistry and Catalysis*; Wiley: New York, 1994.
(16) Deluga, G. A.; Salge, J. R.; Schmidt, L. D.; Verykios, X. E. *Science* **2004**, *303*, 993−997.
(17) Kim, W. B.; Voitl, T.; Rodriguez-Rivera, G. J.; Dumesic, J. A. *Science* **2004**, *305*, 1280−1283.
(18) Landon, P.; Ferguson, J.; Solsona, B. E.; Garcia, T.; Carley, A. F.; Herzing, A. A.; Kiely, C. J.; Golunskic, S. E.; Hutchings, G. J. *Chem. Commun.* **2005**, 3385−3387.
(19) Groves, J. T.; Quinn, R. *J. Am. Chem. Soc.* **1985**, *107*, 5790−5792.
(20) Valden, M.; Lai, X.; Goodman, D. W. *Science* **1998**, *281*, 1647−1650.
(21) Neumann, R.; Dahan, M. *J. Am. Chem. Soc.* **1998**, *120*, 11969−11976.
(22) Brink, G.-J.; Arends, I. W. C. E.; Sheldon, R. A. *Science* **2000**, *287*, 1636−1639.
(23) Weinstock, I. A.; Barbuzzi, E. M. G.; Wemple, M. W.; Cowan, J. J.; Reiner, R. S.; Sonnen, D. M.; Heintz, R. A.; Bond, J. S.; Hill, C. L. *Nature* **2001**, *414*, 191−195.
(24) Boring, E.; Geletii, Y. V.; Hill, C. L. *J. Am. Chem. Soc.* **2001**, *123*, 1625−1635.
(25) Rhule, J. T.; Neiwert, W. A.; Hardcastle, K. I.; Do, B. T.; Hill, C. L. *J. Am. Chem. Soc.* **2001**, *123*, 12101−12102.
(26) Boring, E.; Geletii, Y.; Hill, C. L. In *Catalytic Activation of Dioxygen*; Simandi, L. I., Ed.; Kluwer: Dordrecht, 2001.
(27) Dijksman, A.; Marino-González, A.; Payeras, A. M. i.; Arends, I. W. C. E.; Sheldon, R. A. *J. Am. Chem. Soc.* **2001**, *123*, 6826−6833.
(28) Porta, F.; Rossi, M. *J. Mol. Catal. A: Chem.* **2003**, *204*−*205*, 553−559.
(29) Chen, M. S.; Goodman, D. W. *Science* **2004**, *306*, 252−255.
(30) Sanchez-Castillo, M. A.; Couto, C.; Kim, W. B.; Dumesic, J. A. *Angew. Chem., Int. Ed.* **2004**, *43*, 1140−1140.
(31) Bar-Nahum, I.; Khenkin, A. M.; Neumann, R. *J. Am. Chem. Soc.* **2004**, *126*, 10236−10237.
(32) Neumann, R. In *Transition Metals for Organic Synthesis*, 2nd ed.; Beller, M.; Bolm, C.; Eds.; Wiley-VCH: Weinheim, 2004; Vol. 2, pp 415−426.
(33) Choudhary, T. V.; Goodman, D. W. *Appl. Catal. A: Gen.* **2005**, *291*, 32−36.
(34) *Catalysis by Gold*; Hutchings, G. J.; Haruta, M., Eds.; Elsevier: New York, 2005; Vol. 291.
(35) Hutchings, G. J.; Haruta, M. *Appl. Catal. A: Gen.* **2005**, *291*, 2−5.
(36) Okun, N. M.; Tarr, J. C.; Hilleshiem, D. A.; Zhang, L.; Hardcastle, K. I.; Hill, C. L. *J. Mol. Catal. A. Chem.* **2006**, *246*, 11−17.
(37) Hill, C. L.; Anderson, T. M.; Han, J.; Hillesheim, D. A.; Geletii, Y. V.; Okun, N. M.; Cao, R.; Botar, B.; Musaev, D. G.; Morokuma, K. *J. Mol. Catal. A. Chem.* **2006**, *251*, 234−238.
(38) Glueck, D. S.; Wu, J.; Hollander, F. J.; Bergman, R. G. *J. Am. Chem. Soc.* **1991**, *113*, 2041−2054.
(39) Andrews, M. A.; Gould, G. L.; Voss, E. J. *Inorg. Chem.* **1996**, *35*, 5740−5742.
(40) Verma, A. K.; Lee, S. C. *J. Am. Chem. Soc.* **1999**, *121*, 10838−10839.
(41) Verma, A. K.; Nazif, T. N.; Achim, C.; Lee, S. C. *J. Am. Chem. Soc.* **2000**, *122*, 11013−11014.
(42) Mindiola, D. J.; Hillhouse, G. L. *J. Am. Chem. Soc.* **2001**, *123*, 4623−4624.
(43) Melenkivitz, R.; Mindiola, D. J.; Hillhouse, G. L. *J. Am. Chem. Soc.* **2002**, *124*, 3846−3847.
(44) Mindiola, D. J.; Hillhouse, G. L. *J. Am. Chem. Soc.* **2002**, *124*, 9976−9977.
(45) Artero, V.; Proust, A.; Herson, P.; Villain, F.; Moulin, C. C. d.; Gouzerh, P. *J. Am. Chem. Soc.* **2003**, *125*, 11156−11157.
(46) Thyagarajan, S.; Shay, D. T.; Incarvito, C. D.; Rheingold, A. L.; Theopold, K. H. *J. Am. Chem. Soc.* **2003**, *125*, 4440−4441.
(47) Waterman, R.; Hillhouse, G. L. *J. Am. Chem. Soc.* **2003**, *125*, 13350−13351.
(48) Hu, X.; Meyer, K. *J. Am. Chem. Soc.* **2004**, *126*, 16322−16323.
(49) MacBeth, C. E.; Thomas, J. C.; Betley, T. A.; Peters, J. C. *Inorg. Chem* **2004**, *43*, 4645−4662.
(50) Seo, M. S.; In, J.-H.; Kim, S. O.; Oh, N. Y.; Hong, J.; Kim, J.; Que, Jr., L.; Nam, W. *Angew. Chem., Int. Ed.* **2004**, *43*, 2417−2420.
(51) Amisial, L. D.; Dai, X.; Kinney, R. A.; Krishnaswamy, A.; Warren, T. H. *Inorg. Chem.* **2004**, *43*, 6537−6539.
(52) Dai, X.; Warren, T. H. *J. Am Chem. Soc.* **2004**, *126*, 10085−10094.
(53) Kogut, E.; Zeller, A.; Warren, T. H.; Strassner, T. *J. Am. Chem. Soc.* **2004**, *126*, 11984−11994.
(54) Larsen, P. L.; Gupta, R.; Powell, D. R.; Borovik, A. S. *J. Am. Chem. Soc.* **2004**, *126*, 6522−6523.
(55) Klinker, E. J.; Kaizer, J.; Brennessel, W. W.; Woodrum, N. L.; Cramer, C. J.; Que, Jr., L. *Angew. Chem., Int. Ed.* **2005**, *44*, 3690−3694.
(56) Rohde, J.-U.; Que, Jr., L. *Angew. Chem., Int. Ed.* **2005**, *44*, 2255−2258.
(57) Kogut, E.; Wiencko, H. L.; Zhang, L.; Cordeau, D. E.; Warren, T. H. *J. Am. Chem. Soc.* **2005**, *127*, 11248−11249.
(58) Abu-Omar, M. M.; Loaiza, A.; Hontzeas, N. *Chem. Rev.* **2005**, *105*, 2227−2252.
(59) Berry, J. F.; Bill, E.; Bothe, E.; George, S. D.; Mienert, B.; Neese, F.; Wieghardt, K. *Science* **2006**, *312*, 1937−1941.
(60) Badiei, Y. M.; Krishnaswamy, A.; Melzer, M. M.; Warren, T. H. *J. Am. Chem. Soc.* **2006**, *128*, 15056−15057.
(61) Dey, A.; Hocking, R. K.; Larsen, P.; Borovik, A. S.; Hodgson, K. O.; Hedman, B.; Solomon, E. I. *J. Am. Chem. Soc.* **2006**, *128*, 9825−9833.
(62) Khenkin, A. M.; Kumar, D.; Shaik, S.; Neumann, R. *J. Am. Chem. Soc.* **2006**, *128*, 15451−15460.
(63) Thomas, C. M.; Mankad, N. P.; Peters, J. C. *J. Am. Chem. Soc.* **2006**, *128*, 4956−4957.
(64) Klinker, E. J.; Jackson, T. A.; Jensen, M. P.; Stubna, A.; Juhász, G.; Bominaar, E. L.; Münck, E.; Que, Jr., L. *Angew. Chem., Int. Ed.* **2006**, *45*, 7394−7397.
(65) Cowley, R. E.; Bontchev, R. P.; Sorrell, J.; Sarracino, O.; Feng, Y.; Wang, H.; Smith, J. M. *J. Am. Chem. Soc.* **2007**, *129*, 2424−2425.
(66) Oliveira, F. T. d.; Chanda, A.; Banerjee, D.; Shan, X.; Mondal, S.; Que, Jr., L.; Bominaar, E. L.; Münck, E.; Collins, T. J. *Science* **2007**, *315*, 835−838.
(67) Ison, E. A.; Cessarich, J. E.; Travia, N. E.; Fanwick, P. E.; Abu-Omar, M. M. *J. Am. Chem. Soc.* **2007**, *129*, 1167−1178.
(68) Jones, P. G.; Rumpel, H.; Schwarzmann, E.; Sheldrick, G. M.; Paulus, H. *Acta. Crystallogr.* **1979**, *B35*, 1435−1437.
(69) *Gold: Progress in Chemistry, Biochemistry and Technology*; Schmidbaur, H., Ed.; John Wiley & Sons, Ltd.: Chichester, West Sussex, 1999.
(70) Szuromi, E.; Hui, S.; Sharp, P. R. *J. Am. Chem. Soc.* **2003**, *124*, 10522−10523.
(71) Singh, A.; Sharp, P. R. *Dalton Trans.* **2005**, 2080−2081.
(72) Cinellu, M. A.; Minghetti, G.; Pinna, M. V.; Stoccoro, S.; Zucca, A.; Manassero, M. *Chem. Commun.* **1998**, 2397−2398.
(73) Cinellu, M. A.; Minghetti, G.; Pinna, M. V.; Stoccoro, S.; Zucca, A.; Manassero, M.; Sansoni, M. *J. Chem. Soc., Dalton Trans.* **1998**, 1735−1741.
(74) Cinellu, M. A.; Minghetti, G.; Stoccoro, S.; Zucca, A.; Manassero, M. *Chem. Commun.* **2004**, 1618−1619.
(75) Cinellu, M. A.; Minghetti, G.; Cocco, F.; Stoccoro, S.; Zucca, A.; Manassero, M. *Angew. Chem., Int. Ed.* **2005**, *44*, 6892−6895.
(76) Pope, M. T.; Müller, A. *Angew. Chem., Int. Ed.* **1991**, *30*, 34−48.
(77) *Polyoxometalates: From Platonic Solids to Anti-retroviral Activity*; Pope, M. T.; Müller, A., Eds.; Kluwer Academic Publishers: Dordrecht, Netherlands, 1993.
(78) *Polyoxometalate Chemistry From Topology via Self-Assembly to Applications*; Pope, M. T.; Müller, A., Eds.; Kluwer Academic Publishers: Dordrecht, 2001.
(79) *Polyoxometalate Chemistry for Nano-Composite Design*; Yamase, T.; Pope, M. T., Eds.; Kluwer Academic/Plenum Publishers: New York, 2002; Vol. 2.
(80) Borrás-Almenar, J. J.; Coronado, E.; Müller, A.; Pope, M. T. *Polyoxometalate Molecular Science*; Kluwer Academic Publishers: Dordrecht, 2003; Vol. 98.
(81) Pope, M. T. In *Comprehensive Coordination Chemistry II: From Biology to Nanotechnology*; Wedd, A. G., Ed.; Elsevier Ltd.: Oxford, UK, 2004; Vol. 4, pp 635−678.
(82) Hill, C. L. In *Comprehensive Coordination Chemistry-II: From Biology to Nanotechnology*; Wedd, A. G., Ed.; Elsevier Ltd.: Oxford, UK, 2004; Vol. 4, pp 679−759.

$P_2W_{18}O_{68}$].[83,84] This first terminal metal-oxo complex of an element in columns 10−12 of the periodic table forms in aqueous solution in the presence of O_2. It was purified and thoroughly characterized despite being unstable in solution. Subsequent work with an electron-accepting polytungstate that provides steric protection of the terminal metal-oxo moiety by encapsulation in a central cavity permitted isolation and investigation of $K_{10}Na_3[Pd^{IV}(O)(OH)P_2W_{19}O_{69}(OH_2)]$.[85] This bonafide Pd-oxo compound is stable in aqueous solution at appropriate pH values and in the absence of reducing species.

With these recent findings at hand, we questioned whether terminal Au-oxo complexes might exist and be isolable. Such species would be of considerable interest in multiple contexts. Formation of the terminal metal-oxo unit with the coinage metals (Cu, Ag, Au; column 11 elements) should be even more problematical than for Pt and Pd (column 10 elements) because the d-electron counts, and thus metal-terminal oxo antibonding character, may be even higher for the former than for the latter. In addition, considerable recent attention has been focused on O_2-based oxidations catalyzed by metal-oxide-supported Au(0) nanoclusters and films[20,28−30,33−35] because these rival the most active catalysts reported to date for such processes. Cationic Au and in particular terminal Au−O(H) are thought to be the key intermediate in CO and other oxidations catalyzed by metal-oxide-supported gold.[86−88] Despite this interest, there are no molecular (soluble) models of the Au-metal oxide interface or complexes with Au center(s) in metal-oxide-like environments. We report here the synthesis of two terminal Au-oxo complexes that exhibit multiple bonding between Au and oxygen, commensurate with the shortest such bond distances to date, stabilized by electron-poor d^0 redox-active metal-oxide-like polytungstate ligands. The structural, physicochemical, and other properties of these complexes are characterized by more than 10 methods.

Experimental Section

General Methods and Materials. $K_{10}[\alpha_2\text{-}P_2W_{17}O_{61}]\cdot 20H_2O$ (**P_2W_{17}**),[89] $K_{14}[P_2W_{19}O_{69}(OH_2)]\cdot 24H_2O$ (**P_2W_{19}**),[90] $K_{10}[P_2W_{20}O_{70}(OH_2)_2]\cdot 22H_2O$ (**3**),[91] and $K_4H_2[P_2W_{21}O_{71}(OH_2)_3]\cdot 28H_2O$ (**P_2W_{21}**)[92] were synthesized using published procedures. Their purities were confirmed by both IR and ^{31}P NMR. Potassium tungsten oxide (K_2WO_4) and gold chloride ($AuCl_3$) were purchased from Alfa Aesar and were used without further purification. Infrared spectra (2% sample in KBr) were recorded on a Thermo Nicolet 6700 instrument. Ambient temperature electronic absorption spectra were acquired using a diode-array Hewlett-Packard 8452A spectrophotometer (aqueous solution) equipped with a magnetic stirrer and temperature controller (HP 89090A) and a Hitachi U-3501 UV−vis-NIR spectrophotometer using a double-beam configuration at 2.0 nm resolution (butyronitrile solution). ^{31}P NMR measurements were made on a Varian INOVA 400 MHz spectrometer, and peaks were referenced to 85% H_3PO_4. Room-temperature magnetic susceptibilities were measured on a Johnson-Matthey Model MSB-1 magnetic susceptibility balance as neat powders at 24 °C; the balance was calibrated using $Hg[Co(SCN)_4]$ as a standard. Pascal's constants were used to obtain the final diamagnetic corrections. Temperature-dependent magnetic measurements were performed at 0.1 and 1.0 T using a Quantum Design MPMS-5 SQUID magnetometer and employing approximately 80−90 mg of each sample in a cylindrical PTFE-sealed sample holder. Differential scanning calorimetric and thermogravimetric data were collected on Instrument Specialists Incorporated DSC 550 and TGA 1000 instruments, respectively. Electrochemical data were obtained using a BAS CV-50W instrument (Bioanalytical System, Inc.). Elemental analyses of K, P, Au, and W were performed by Desert Analytics (Tucson, Arizona), Kanti Labs (Mississauga, Canada), and Galbraith Laboratories Inc. (Knoxville, TN). The ^{197}Au Mössbauer spectrum of **1** (200 mg sample) measured at 12 K for a week was unsuccessful (showed no signal) because of interference from the tungsten atoms present. The same problem has been documented in attempting to acquire ^{57}Fe Mössbauer spectra of iron-containing polytungstates.[93,94]

Synthesis of $K_{15}H_2[Au(O)(OH_2)P_2W_{18}O_{68}]\cdot 25H_2O$ (1). A 1.20 g (0.25 mmol) sample of $K_{10}[\alpha_2\text{-}P_2W_{17}O_{61}]\cdot 20H_2O$ was dissolved with stirring in 5 mL of deionized water, and the solution was brought to a boil. Potassium tungsten oxide, K_2WO_4 (0.16 g, 0.5 mmol), was then added. The solution was stirred and refluxed for ∼1 d. A 0.38 g (1.25 mmol) sample of gold chloride ($AuCl_3$) was dissolved in 10 mL of water, and the pH of this solution was increased to 6.8 by dropwise addition of 1 M KOH solution. After careful adjustment of the pH value, the Au(III) solution was added to the tungstate solution. The pH of this mixture was then adjusted, again, to 6.8 by dropwise addition of 1 M KOH solution. The mixture was stirred at 60 °C for about 3 h. The clear, orange solution gradually turned dark red over this period. The solution was filtered after it had cooled, and the dark red filtrate afforded, after repeated filtration, deep red, large prismatic crystals of **1** (0.50 g, yield 36%, based on P). The crystals were removed from the solution by filtration and dried under suction for 12 h. Analytical data: IR (2% KBr pellet, 1300−400 cm^{-1}): 1073 (s), 1019 (m), 963 (sh), 939 (s), 893 (m), 852 (sh), 831 (s), 750 (s), 619 (s), 508 (m). ^{31}P NMR (8 mM solution in D_2O): −8.7 ppm ($\Delta\nu_{1/2}$ = 8 Hz). Electronic spectral data (400−800 nm, in H_2O (1.55 mM sample, 1 cm cell path length)) [λ, nm (ϵ, M^{-1} cm^{-1})]: 402 nm (552) and 428 nm (312). Magnetic susceptibility (0.1 and 1.0 T; 2−290 K): diamagnetic. Anal. Calcd. for $K_{15}H_2[Au(O)(OH_2)P_2W_{18}O_{68}]\cdot 25H_2O$: K, 10.2; P, 1.1; Au, 3.4; W, 57.8. Found: K, 9.5; P, 1.0; Au, 3.3; W, 57.0. [MW = 5729 g/mol] An organic soluble form, the tetra-*n*-butylammonium (TBA) salt, of **1a** (the polyanion of **1**), was made by extraction of **1** in 1 M KCl aqueous solution, with a dichloromethane solution of 10 equiv of TBACl followed by removal of the dichloromethane solvent. ^{31}P NMR confirmed that there was no decomposition of the polyanion in this ion exchange process (one peak at −15.1 ppm), and thus this hydrophobic salt was used directly in ^{17}O NMR experiments. While addition of *cis*-dicyclohexano-18-crown-6 to solutions of **2** (described in the following paragraph) solubilizes Au-oxo polyanion **2a** in organic solvents, addition of this crown ether to solutions of **1** does not because

(83) Anderson, T. M.; Neiwert, W. A.; Kirk, M. L.; Piccoli, P. M. B.; Schultz, A. J.; Koetzle, T. F.; Musaev, D. G.; Morokuma, K.; Cao, R.; Hill, C. L. *Science* **2004**, *306*, 2074−2077.
(84) Kortz and co-workers (Pd), Cronin and co-workers (Ag) and others have recently reported POM or POM materials containing one or more noble metal centers. For example, see: (a) Reicke, M.; Kortz, U.; Keita, B.; Nadjo, L.; Clark, R. J. *Inorg. Chem.* **2004**, *43*, 3915−3920. (b) Bi, L.-H.; Kortz, U.; Keita, B.; Nadjo, L.; Borrmann, H. *Inorg. Chem.* **2004**, *43*, 8367−8372. (c) Bi, L.-H.; Kortz, U.; Keita, B.; Nadjo, L.; Daniels, L. *Eur. J. Inorg. Chem.* **2005**, 3034−3041. (d) Abbas, H.; Pickering, A. L.; Long, D.-L.; Kögerler, P.; Cronin, L. *Chem. Eur. J.* **2005**, *11*, 1071−1078. (e) Pickering, A. L.; Long, D.-L.; Kögerler, P.; Cronin, L. *Inorg. Chem.* **2004**, *43*, 4953−4961. See also reference 25.
(85) Anderson, T. M.; Cao, R.; Slonkina, E.; Hedman, B.; Hodgson, K. O.; Hardcastle, K. I.; Neiwert, W. A.; Wu, S.; Kirk, M. L.; Knottenbelt, S.; Depperman, E. C.; Keita, B.; Nadjo, L.; Musaev, D. G.; Morokuma, K.; Hill, C. L. *J. Am. Chem. Soc.* **2005**, *127*, 11948−11949.
(86) Bond, G. C.; Thompson, D. T. *Gold Bull.* **2000**, *33*, 41−51.
(87) Guzman, J.; Gates, B. C. *J. Am. Chem. Soc.* **2004**, *126*, 2672−2673.
(88) Henao, J. D.; Caputo, T.; Yang, J. H.; Kung, M. C.; Kung, H. H. *J. Phys. Chem. B* **2006**, *110*, 8689−8700.
(89) Contant, R. In *Inorganic Syntheses*; Ginsberg, A. P., Ed.; John Wiley and Sons: New York, 1990; Vol. 27, pp 104−111.
(90) Tourné, C. M.; Tourné, G. F. *J. Chem. Soc., Dalton Trans.* **1988**, 2411−2420.
(91) Contant, R. *Can. J. Chem.* **1987**, *65*, 568−573.
(92) Tourné, C. M.; Tourné, G. F.; Weakley, T. J. R. *J. Chem. Soc., Dalton Trans.* **1986**, 2237−2242.
(93) Zhang, X.; Chen, Q.; Duncan, D. C.; Campana, C.; Hill, C. L. *Inorg. Chem.* **1997**, *36*, 4208−4215.
(94) Zhang, X.; Chen, Q.; Duncan, D. C.; Lachicotte, R. J.; Hill, C. L. *Inorg. Chem.* **1997**, *36*, 4381−4386.

Table 1. Crystal Data and Refinement Parameters for the X-ray Structures of $K_{15}H_2[Au(O)(OH_2)P_2W_{18}O_{68}]\cdot 25H_2O$ (**1**) (Datasets at Both 173(2) K and 96(2) K) and $K_7H_2[Au(O)(OH_2)P_2W_{20}O_{70}(OH_2)_2]\cdot 27H_2O$ (**2**)

	1 (173(2) K)	**1** (96(2) K)	**2**
molecular formula	$H_{54}K_{15}O_{95}P_2AuW_{18}$	$H_{54}K_{15}O_{95}P_2AuW_{18}$	$H_{62}K_7O_{101}P_2AuW_{20}$
formula wt. (g mol^{-1})	5729.14	5729.14	5887.80
temperature (K)	173(2)	96(2)	173(2)
radiation (λ, Å)	0.71073	0.71073	0.71073
crystal system	orthorhombic	orthorhombic	hexagonal
space group	*Fddd* (no. 70)	*Fddd* (no. 70)	*P*6(3)/*mmc* (no. 194)
a (Å)	28.594(4)	28.605(5)	16.1730(9)
b (Å)	31.866(4)	31.857(5)	16.1730(9)
c (Å)	38.241(5)	38.273(6)	19.7659(15)
volume (Å^3)	34844(7)	34876(10)	4477.4(5)
Z	16	16	2
ρ_{calcd} (g cm^{-3})	4.368	4.364	4.198
μ (mm^{-1})	26.219	25.902	27.713
F(000)	40640	37760	4956
crystal size (mm^3)	0.25 × 0.23 × 0.20	0.45 × 0.44 × 0.28	0.33 × 0.28 × 0.17
reflections collected	118464	56787	59942
independent reflections	10902 [R(int) = 0.0823]	10824 [R(int) = 0.1047]	2107 [R(int) = 0.0697]
absorption correction	semiempirical from equivalents	SADABS and face index	semiempirical from equivalents
refinement method	full-matrix least-squares on F^2	full-matrix least-squares on F^2	full-matrix least-squares on F^2
goodness-of-fit on F^2	1.048	1.046	1.248
final *R* indices	$R_1{}^a = 0.0540$	$R_1{}^a = 0.0554$	$R_1{}^a = 0.0634$
[$R > 2\sigma$ (I)]	$wR_2{}^b = 0.2293$	$wR_2{}^b = 0.1245$	$wR_2{}^b = 0.2677$
R indices (all data)	$R_1{}^a = 0.0628$	$R_1{}^a = 0.0932$	$R_1{}^a = 0.0639$
	$wR_2{}^b = 0.2410$	$wR_2{}^b = 0.1320$	$wR_2{}^b = 0.2683$
largest diff. peak and hole (e Å^{-3})	5.508 and −8.046	5.644 and −4.069	11.568 and −6.549

[a] $R_1 = \Sigma||F_o| - |F_c||/|F_o|$. [b] $wR_2 = \{\Sigma[w(F_o{}^2 - F_c{}^2)^2]/\Sigma[w(F_o{}^2)^2]\}^{0.5}$.

1a bears a 17− charge while **2a** bears only a 9− charge. In addition, TBABr cannot be used in place of TBACl in the metathesis extraction because **1a** (and **2a**) are reduced by bromide.

Synthesis of $K_7H_2[Au(O)(OH_2)P_2W_{20}O_{70}(OH_2)_2]\cdot 27H_2O$ (2). A 1.00 g (0.176 mmol) sample of $K_{10}[P_2W_{20}(OH_2)_2O_{70}]\cdot 22H_2O$ was dissolved in 5 mL of deionized water at room temperature, and 0.27 g (0.890 mmol) of gold chloride ($AuCl_3$) was added to the clear, colorless solution with stirring. The red-orange mixture was stirred at 55 °C for about 2 h and gradually turned dark red over this period. The hot solution was cooled to room temperature and then filtered through VWR 410 qualitative filter paper (porosity 0.45 μm). The large, red crystals of **2** normally appear in 2 d if the solution is allowed to stand in air at room temperature (0.80 g, yield 78%, based on P). The crystals were removed from the solution by filtration and dried under suction for 12 h. Analytical data: IR (2% KBr pellet, 1300−400 cm^{-1}): 1089 (s), 1032 (s), 963 (s), 942 (m), 855 (sh), 755 (s), 698 (m), 660 (sh), 602 (sh), 525 (m). ^{31}P NMR (10 mM solution in D_2O): −13.15 ppm ($\Delta\nu_{1/2} = 8$ Hz). Electronic spectral data (400−800 nm, in H_2O (1.65 mM sample, 1 cm cell path length)) [λ, nm (ϵ, M^{-1} cm^{-1})]: 402 nm (485) and 428 nm (295). Magnetic susceptibility (0.1 and 1.0 T; 2−290 K): diamagnetic. Anal. Calcd. for $K_7H_2[Au(O)(OH_2)P_2W_{20}O_{70}(OH_2)_2]\cdot 27H_2O$: K, 4.6; P, 1.0; Au, 3.3; W, 62.5. Found: K, 4.5; P, 1.0; Au, 3.2; W, 61.9 [MW = 5888 g/mol]. An organic soluble form, the K⊂*cis*-dicyclohexano-18-crown-6 salt, of **2a** (the polyanion of **2**) was made by adding 5 equiv of *cis*-dicyclohexano-18-crown-6 to an acetonitrile solution of **2**. ^{31}P NMR confirmed that treatment with *cis*-dicyclohexano-18-crown-6 produced no detectable decomposition of the polyanion (−15.5 ppm), and thus this hydrophobic salt was used directly in ^{17}O NMR experiments including oxo transfer reactivity.

Optical Spectroscopy at 17K. These spectra were collected using a Janis STVP-100 continuous flow cryostat mounted in a custom-designed cradle assembly, and the sample temperature was monitored with a Lakeshore silicon-diode (PT-470). The sample was dissolved in a 1:3 water:glycerol mixture in order to obtain a good optical glass. The resulting solution was injected through a rubber gasket spacer (approximately 1 mm thick) between two 1-mm thick Infrasil quartz discs in a custom-designed sample holder. Gaussian resolution of spectral bands was accomplished using GRAMS AI software.

X-ray Crystallographic Studies. (a) Instrumentation and Methods. The complete datasets for **1**, **2**, and **3** were collected at Emory University (Table 1). Single crystals of $K_{15}H_2[Au(O)(OH_2)P_2W_{18}O_{68}]\cdot 25H_2O$ (**1**), $K_7H_2[Au(O)(OH_2)P_2W_{20}O_{70}(OH_2)_2]\cdot 27H_2O$ (**2**), and $K_{10}[P_2W_{20}O_{70}(OH_2)_2]\cdot 22H_2O$ (**3**), suitable for X-ray analysis, were each coated with Paratone-N oil, suspended in a small fiber loop, and placed in a cooled gas stream on a Bruker D8 SMART APEX CCD sealed tube diffractometer. Diffraction intensities were measured using graphite monochromated Mo Kα radiation ($\lambda = 0.71073$ Å) at 173(2) K and a combination of φ and ω scans with 10 s frames traversing about ω at 0.3° increments. In addition, a second dataset for compound **1** was collected at 96(2) K. Data collection, indexing, and initial cell refinements were carried out using SMART;[95] frame integration and final cell refinements were done using SAINT.[96] The molecular structure of each complex was determined using Direct Methods and Fourier techniques and refined by full-matrix least-squares.[97] A multiple absorption correction for each dataset at 173(2) K was applied using the program SADABS,[98] while face-indexed absorption correction was applied for the dataset of **1** at 96(2) K. The largest residual electron density for each structure was located close to (less than 1.0 Å from) the W, Au, and K atoms and was most likely due to imperfect absorption corrections frequently encountered in heavy-metal atom structures.

(b) Refinement Details. The structures of **1**, **2**, and **3** were solved using Direct Methods and difference Fourier techniques.[97] The K, P, W, Au atoms in **1** were refined anisotropically. Some of the potassium ions and solvent water molecules were refined with partial occupancies; not all the countercations and solvent water molecules could be located in difference Fourier maps because of disorder. Scattering factors and anomalous dispersion corrections are taken from the *International Tables for X-ray Crystallography*. Structure solution, refinement, graphics, and generation of publication materials were performed by using SHELXTL, V6.14 software.

(95) SMART, Bruker AXS, I.; 5.628 ed.; Analytical X-ray Systems: Madison, WI, 2003.
(96) SAINT, Bruker AXS, I.; 6.28 ed.; Analytical X-ray Systems: Madison, WI, 2003.
(97) SHELXTL; 6.14 ed.; Bruker AXS, Inc.: Madison, WI, 2003.
(98) SADABS, Sheldrick, G.; 2.10 ed. 2003.

Neutron Diffraction Studies. (a) Neutron Data Collection. Neutron diffraction data were obtained at the Intense Pulsed Neutron Source (IPNS) at Argonne National Laboratory using the time-of-flight Laue single-crystal diffractometer (SCD).[99] A crystal of $K_{15}H_2[Au(O)(OH_2)P_2W_{18}O_{68}]\cdot 25H_2O$ (**1**), approximately 15 mm^3 in volume and weighing 60 mg, was coated in fluorocarbon grease, wrapped in aluminum foil, and glued to an aluminum pin that was mounted on the cold stage of a closed-cycle helium refrigerator. The crystal was then cooled to 30 ± 1 K. The unit cell approximately matched the X-ray unit cell, indicating that the neutron sample was the correct material. Intensities were integrated about their predicted locations and were corrected for the Lorentz factor, the incident spectrum, and the detector efficiency. A wavelength-dependent spherical absorption correction was applied using cross sections from Sears[100a] for the nonhydrogen atoms and from Howard et al.[100b] for the hydrogen atoms (μ (cm^{-1}) = 0.540 + 0.405 λ). Symmetry-related reflections were not averaged since different extinction factors are applicable to reflections measured at different wavelengths. All other details on the neutron diffraction studies are given in the Supporting Information (SI).

(b) Refinement. The GSAS software package was used for structural analysis.[101] The atomic positions of the potassium cations and the $[Au(O)(OH_2)P_2W_{18}O_{68}]$ core of the molecule from the X-ray diffraction structure were used as an initial model to phase the neutron data. Lattice water molecules were located from difference Fourier syntheses. Each of the oxygen atoms attributable to lattice water was associated with strong negative scattering-density peaks, which are indicative of hydrogen atoms. For these peaks that were assigned as hydrogen atoms, subsequent refinement showed significant fractional occupancy and supported their interpretation as "real" atoms. Atom positions from the original X-ray structure that did not appear to have any weight in the neutron structure were omitted from the model. The axial water ligand O1W, bound to Au *trans* to the O35 oxo ligand, appeared to be disordered. A large area of negative density was located close to this oxygen on the O35−Au−O1W axis; other areas of negative density were located off this axis and also close to O1W, indicative that O1W is indeed a water molecule bound to Au. The hydrogen atoms bound to O1W were not included in the refinement. No such area of negative scattering density was located about the O35 oxo ligand. The refinement was based on F^2 reflections with a minimum d-spacing of 1.0 Å. Weights were assigned as $w(F_o^2) = 1/[(\sigma^2(F_o^2)]^2$ where $\sigma^2(F_o^2)$ is the variance based on counting statistics. In the final refinement, all atoms, including hydrogen atoms, were refined with isotropic displacement parameters. After final refinement the maximum residual peak height in the difference Fourier map was 0.210 fm $Å^{-3}$, which corresponds to approximately 10% of the peak height observed for atom O35 in the Fourier map. Data collection and refinement parameters are summarized in Table 2 and bond distances and angles for the [Au−O_6] octahedral core are included in Table 3.

pH Dependent UV−vis Titrations of 2. The pH titrations of **2** were performed in two opposite directions. (1) A 0.2082 g sample of **2** was dissolved in 10 mL of deionized water (3.54 mM, the initial pH was 2.95). The pH was lowered to 0.38 by dropwise addition of 0.1 M HCl and then increased again to the initial value by dropwise addition of 0.1 M NaOH. (2) A 0.1059 g sample of **2** was dissolved in 10 mL of deionized water (1.80 mM, the initial pH was 3.21). The pH was increased to 7.53 by dropwise addition of 0.1 M NaOH and then lowered again to the initial value by dropwise addition of 0.1 M HCl. UV−vis spectra were taken after each change of pH by *ca.* 0.25 units.

Electrochemistry. Cyclic voltammograms (CV) were obtained at room temperature with scan rates in the range 2−100 mV/s. All reduction potentials are given versus Ag/AgCl (3 M NaCl) reference electrode ($E_{NHE} = E_{Ag/AgCl}$ + 0.250 V at 25 °C). A coiled Pt-wire was used as an auxiliary electrode. A glassy carbon working electrode was always polished with alumina (Polishing Alumina Fluid, purchased from Bioanalytical Systems, Inc.) before use unless otherwise specified. Bulk electrolysis was performed under argon on a reticulated vitreous carbon working electrode with a coiled Pt-wire as an auxiliary electrode within a fritted glass isolated chamber. Vigorous agitation was provided by a magnetic stirrer and by the passing of argon as a purging gas. Air was rigorously excluded at all times. The total coulombs passed were monitored continuously. All details are given in the SI.

Table 2. Crystal Data and Structural Refinement for the Neutron Diffraction Structure of $K_{15}H_2[Au(O)(OH_2)P_2W_{18}O_{68}]\cdot 25H_2O$ (**1**)

formula	$H_{54}K_{15}O_{95}P_2AuW_{18}$
formula wt. (g mol^{-1})	5728.82
temperature (K)	30(1)
crystal system	orthorhombic
space group	*Fddd* (no. 70)
a (Å)	28.72(2)
b (Å)	31.61(4)
c (Å)	39.16(1)
V ($Å^3$)	35555(51)
Z	16
d_{calc} (g cm^{-3})	4.003
size (mm^3)	15
radiation	neutrons
data collection technique	time-of-flight Laue
$\mu(\lambda)$, cm^{-1}	0.540 + 0.405λ
max, min transmission	0.8455, 0.4038
extinction parameter	$1.2(1) \times 10^{-3}$
d_{min} (Å)	1.0
no. of reflections	3435
no. of reflections ($I > 3\sigma(I)$)[a]	2988
no. of parameters refined	306
refinement method	full-matrix least-squares on F^2
R indices $R_w(F^2)$,[b] $R(F^2)$[c]	0.186, 0.192
R indices $R_w(F)$,[d] $R(F)$[e]	0.105, 0.132
goodness-of-fit	2.99

[a] Outliers with $|(F_o^2 - F_c^2)|/\sigma F_o^2 > 6$ were rejected. [b] $R_w(F^2) = \{\Sigma[w(F_o^2 - F_c^2)^2]/\Sigma[w(F_o^2)^2]\}^{1/2}$. [c] $R(F^2) = \Sigma|F_o^2 - F_c^2|/\Sigma|F_o^2|$. [d] $R_w(F) = \{\Sigma[w(|F_o| - |F_c|)^2]/\Sigma[w(|F_o|)^2]\}^{1/2}$. [e] $R(F) = \Sigma||F_o| - |F_c||/\Sigma|F_o|$.

Chemical Titrations. The stoichiometry of the reaction of **2** with 2,2′-azino-bis(3-ethylbenzothiazoline-6-sulfonic acid) ($ABTS^{2-}$) (ammonium salt, Aldrich, 98%) or $Fe^{II}(CN)_6^{4-}$ (potassium salt, Aldrich, 99%) was determined using electronic absorption spectroscopy. In addition, **2** was also titrated potentiometrically with standardized $SiW_{12}O_{40}^{5-}$ (or $AlW_{12}O_{40}^{6-}$) solutions under argon using a platinum VWR symphony combination redox electrode. All details are given in the SI.

X-ray Absorption Spectroscopy Studies. All samples were prepared as finely ground solids in boron nitride, pressed into a pellet, and sealed between 38 μm Kapton tape windows in a 1-mm thick aluminum spacer. The X-ray absorption spectra were measured at the Stanford Synchrotron Radiation Laboratory (SSRL) on the unfocused bend magnet beam line 2−3 for Au(III) samples, and the wiggler beam line 9−3 for Au(I) samples, with the ring operating at 3 GeV, 85−100 mA. A water-cooled (beam line 2−3) and liquid-nitrogen cooled (beam line 9−3) Si(220) monochromator was utilized for energy selection at the Au L_2 edge. At beam line 2−3, the monochromator was detuned 50% at 14340 eV to minimize higher harmonic components in the X-ray beam. At beam line 9−3, a collimating pre-monochromator mirror was used for harmonic rejection with the monochromator fully tuned. The data were measured in transmission mode for gold(III) acetate, gold(I) potassium cyanide, and gold(I) sodium thiosulfate, and in fluorescence mode for gold-containing polyoxometalate samples, using a Canberra 13-element solid-state germanium detector. For transmission measurements, the internal energy calibrations were performed by simultaneous measurement of the absorption of a reference Au foil placed between two ionization chambers located after the sample. For fluorescence data, the spectrum of the Au foil was collected between the data scans. The first inflection point of the foil was assigned to 13734.0 eV. The sample

(99) Schultz, A. J.; De Lurgio, P. M.; Hammonds, J. P.; Mikkelson, D. J.; Mikkelson, R. L.; Miller, M. E.; Naday, I.; Peterson, P. F.; Porter, R. R.; Worlton, T. G. *Physica B* **2006**, *385−386*, 1059−1061.
(100) (a) Sears, V. F. In *Methods of Experimental Physics*; Academic Press: Orlando, FL, 1986; Vol. 23, pp 521−550. (b) Howard, J. A. K.; Johnson, O.; Schultz, A. J.; Stringer, A. M. *J. Appl. Crystallogr.* **1987**, *20*, 120−122.
(101) Larson, A. C.; Von Dreele, R. B. *General Structure Analysis System (GSAS)*; Los Alamos National Laboratory Report LAUR 86−748, 2004.

Table 3. Bond Distances (Å) and Angles (deg) for the [Au−O_6] Octahedral Core as Derived from Neutron Diffraction Data

atoms	distances or angles	atoms	distances or angles
Au1−O35	1.771(22)	Au1−O32*	1.893(12)
Au1−O1W	1.983(28)	Au1−O34	1.901(11)
Au1−O32	1.893(12)	Au1−O34*	1.901(11)
O32−Au1−O32*	163.3(11)	O32*−Au1−O1W	81.7(6)
O32−Au1−O34	89.1(5)	O34−Au1−O34*	164.9(11)
O32−Au1−O34*	88.7(5)	O34−Au1−O35	97.6(6)
O32−Au1−O35	98.3(6)	O34−Au1−O1W	82.4(6)
O32−Au1−O1W	81.7(6)	O34*−Au1−O35	97.6(6)
O32*−Au1−O34	88.7(5)	O34*−Au1−O1W	82.4(6)
O32*−Au1−O34*	89.1(5)	O35−Au1−O1W	180.0
O32*−Au1−O35	98.3(6)		

was maintained at 12 K using an Oxford Instruments CF1208 continuous-flow liquid helium cryostat. A total of two to six scans to a k value of 9.5−12.5 $Å^{-1}$ were collected for each sample. The edge features were monitored for photoreduction; no change was observed in any of the samples. The data were normalized using the program XFIT[102] by first subtracting a polynomial background absorbance that was fit to the preedge region and extended over the postedge with control points, followed by fitting a two-region polynomial spline of orders 2 and 3 over the postedge region. The data were normalized to an edge jump of 1.0 between the background and spline curves at 13750.0 eV.

^{17}O NMR Experiments. (a) General Methods and Materials. ^{17}O NMR spectra were acquired at 81.291 MHz on a Varian UNITY 600 spectrometer. The spectrometer was locked on the ^{2}H resonance of $CDCl_3$, and all chemical shifts were reported relative to D_2O ($\delta = 0$ ppm). Spectral parameters for ^{17}O NMR were the following: pulse width, 10 μs; sweep width, 100 000 Hz; 0.01 s delay; 100 000 transients; 40 000 data points. Spectra were obtained using cylindrical 5-mm o.d. sample tubes (7 in). All samples were dissolved in 50:50 (v:v) CH_3CN−$CDCl_3$ mixture solvent at room temperature. ^{17}O-enriched water (10% $H_2{}^{17}O$) was purchased from Cambridge Isotope Laboratories and was used without further purification. Tetra-*n*-butylammonium (TBA) chloride and *cis*-dicyclohexano-18-crown-6 were purchased from Aldrich and were used without further purification.

(b) ^{17}O Enrichment of $K_{15}H_2[Au(O)(OH_2)P_2W_{18}O_{68}]\cdot 25H_2O$ (1). The preparation of an organic soluble salt of **1a**, polyanion of **1**, was described above. An exemplary procedure is as follows: a 0.20 g (0.036 mmol) sample of **1** was suspended in 2 mL of 1 M aqueous KCl solution, and then a 20 mL solution of $[CH_3(CH_2)_3]_4NCl$ (TBACl, 0.10 g, 0.36 mmol) in CH_2Cl_2 was added quickly with vigorous stirring at room temperature. Upon standing, the mixture separated into a clear yellow organic layer and a cloudy white aqueous layer. The organic layer was separated and filtered using a 0.45-μm nylon membrane filter and then was concentrated to dryness at room temperature using a rotary evaporator. The resulting solids were dissolved in 1.0 mL of CH_3CN (the purity was checked by ^{31}P NMR; the spectrum had only one peak at −15.1 ppm in $CH_3CN/CDCl_3$ solvent). A 0.10 mL sample of 10% ^{17}O-enriched water was added to this CH_3CN solution and the mixture was kept for 2 d at 50 °C. The mixture was then concentrated using a rotary evaporator, and the resulting solids were redissolved in 0.5 mL of $CH_3CN/ CDCl_3$.

(c) ^{17}O Enrichment of $K_7H_2[Au(O)(OH_2)P_2W_{20}O_{70}(OH_2)_2]\cdot 27H_2O$ (2). Two methods were used to obtain ^{17}O-enriched **2** in an organic solvent. Method 1: a 0.20 g (0.036 mmol) sample of **2** was dissolved in 0.30 mL of 10% ^{17}O-enriched water and incubated at 50 °C for 2 d. This solution was then concentrated to dryness at room temperature using a rotary evaporator. A 0.067 g (0.18 mmol) sample of *cis*-dicyclohexano-18-crown-6 was added to the dried solids of **2**, and the mixture was redissolved in 0.5 mL of $CH_3CN/CDCl_3$ at room temperature. The purity was checked by ^{31}P NMR; the spectrum had only one peak at −15.5 ppm. Method 2: a 0.20 g (0.036 mmol) sample of **2** was dissolved at room temperature in 2.0 mL of CH_3CN containing 0.067 g (0.18 mmol) of *cis*-dicyclohexano-18-crown-6 and then 0.20 mL of 10% ^{17}O-enriched water was added. The mixture was incubated at room temperature for 2 d. This solution was then concentrated to dryness at room temperature, affording the K⊂*cis*-dicyclohexano-18-crown-6 salt of **2**. The dried solid was redissolved in 0.5 mL of $CH_3CN/CDCl_3$, and its purity was checked by ^{31}P NMR; the spectrum had only one peak at −15.5 ppm.

(d) Oxo Transfer to Ph_3P. Argon was bubbled for 15 min through *ca.* 1 mL of $CH_3CN/CDCl_3$ containing 0.20 g (0.034 mmol) of ^{17}O-enriched sample of **2** in a cylindrical 5-mm o.d. sample tube (7 in), and then a 9.2 mg (0.035 mmol) sample of triphenylphosphine was added quickly. After addition of triphenylphosphine, the NMR tube was immediately sealed, and a ^{31}P NMR spectrum was taken in *ca.* 2 min. The mixture was allowed to react at least 1 h at room temperature for complete conversion. The mixture was subsequently analyzed by ^{31}P and ^{17}O NMR spectroscopy. The reaction was also carried out with 3 (27.6 mg, 0.105 mmol) or 5 (46.0 mg, 0.175 mmol) equiv of triphenylphosphine over **2**.

Computational Methods. In these calculations we used SDD basis sets and ECP for Au[103−105] and the aug-cc-pVTZ basis set for the O[106,107] atoms. B3LYP calculations were done using the GAUSSIAN_2003 quantum chemical package.[108] In the Complete Active-State Self-Consistent Field (CASSCF) calculations on the small models, an active space that included all valence electrons and orbitals from the Au and O atoms was used: for AuO this is a 17 electron/10 orbital active space, referred to as (17/10), for AuO^+ this is a (16/10) active space, for AuO^{2+} this is a (15/10) active space, and for AuO^{3+} this is a (14/10) active space. All CASSCF and Multi-Reference Single-Double Correlation Interaction (MRSD-CI) calculations were performed by the MOLPRO quantum chemical package.[109]

Results

Synthesis of Terminal Au-Oxo Complexes 1 and 2. Successful preparation of the Pt-oxo complex, $K_7Na_9[Pt^{IV}O(OH_2)P_2W_{18}O_{68}]$,[83] and Pd-oxo complex, $K_{10}Na_3[Pd^{IV}O(OH)P_2W_{19}O_{69}(OH_2)]$,[85] using $[A\text{-}PW_9O_{34}]^{9-}$ as an inorganic ligand encouraged us to use a similar strategy to synthesize analogous Au-oxo compounds. We rationalized that empty electron-withdrawing delocalized metal-based orbitals in the d^0 $[A\text{-}PW_9O_{34}]^{9-}$ might match in energy the d orbitals on the coordinated metal (Au) reasonably well and thus might stabilize a Au-oxo unit

(102) Ellis, P. J.; Freeman, H. C. *J. Synchrotron Radiat.* **1995**, 190−195.
(103) Haeussermann, U.; Dolg, M.; Stoll, H.; Preuss, H. *Mol. Phys.* **1993**, *78*, 1211−1224.
(104) Dolg, M.; Stoll, H.; Preuss, H.; Pitzer, R. M. *J. Phys. Chem.* **1993**, *97*, 5852−5859.
(105) Dolg, M.; Stoll, H.; Preuss, H. *Theor. Chim. Act.* **1993**, *85*, 441−450.
(106) Kendall, R. A.; Dunning, Jr., T. H.; Harrison, R. J. *J. Chem. Phys.* **1992**, *96*, 6796−6806.
(107) Woon, D. E.; Dunning, Jr., T. H. *J. Chem. Phys.* **1993**, *98*, 1358−1371.
(108) Frisch, M. J. et al., 03 Rev. C1 ed.; Gaussian, Inc.: Pittsburgh, 2003.
(109) MOLPRO, Werner, H. J.; Knowles, P. J. 2003.

by withdrawal of antibonding as well as bonding electron density in this unit. Direct addition of the sodium salt of $[A\text{-}PW_9O_{34}]^{9-}$ to different Au(III) solutions, including potassium tetrachloroaurate ($KAuCl_4$), gold chloride ($AuCl_3$), and gold bromide ($AuBr_3$), followed by kinetic precipitation with KCl always gives the all-tungsten complex, $K_{14}[P_2W_{19}(OH_2)O_{69}]\cdot 24H_2O$ (**P_2W_{19}**), which is the decomposition product of $[A\text{-}PW_9O_{34}]^{9-}$ in aqueous solution.[90] We previously documented that a cocrystalline mixture of **P_2W_{19}** and $[Pd^{II}(OH_2)_2P_2W_{18}O_{68}]^{16-}$ is obtained in acidic Pd(II) media where the decomposition of $[A\text{-}PW_9O_{34}]^{9-}$ is quite rapid.[83] Thus, a stable medium for $[A\text{-}PW_9O_{34}]^{9-}$ appears to be important for successful synthesis of these Au-oxo complexes. Instead of using the solid sodium salt of $[A\text{-}PW_9O_{34}]^{9-}$ as a reactant, we generate this hydrolytically unstable ligand *in situ* by reaction of $K_{10}[\alpha_2\text{-}P_2W_{17}O_{61}]\cdot 20H_2O$ with K_2WO_4 at pH 6.8.[90] ^{31}P NMR studies indicate, however, that direct addition of highly acidic $AuCl_3$ solution (pH 1.2) still causes the decomposition of $[A\text{-}PW_9O_{34}]^{9-}$ (at this stage $[P_2W_{20}(OH_2)_2O_{69}]^{10-}$ is present; characteristic chemical shift, −12.35 ppm). As a result, the pH of this $AuCl_3$ solution is increased to 6.8 by dropwise addition of 1 M KOH before addition to the solution of $[A\text{-}PW_9O_{34}]^{9-}$ generated *in situ*, and the pH of this mixture is carefully maintained at 6.8 with KOH. The orange solution gradually turns dark red with stirring at 60 °C, and its cooled filtrate affords dark red crystals of $K_{15}H_2[Au(O)(OH_2)P_2W_{18}O_{68}]\cdot 25H_2O$ (**1**) in 36% yield.

Significantly, we realized that **1** would not have sufficient stability in solution to facilitate key characterization and reactivity studies (**1** is stable in the solid state, but it readily decomposes in aqueous solution). It was clear we needed to devise ligand systems that would ensure a similar geometrical and electronic structural environment for Au to that experienced by the Au center in **1** yet simultaneously provide much greater hydrolytic stability than that afforded by the $[A\text{-}PW_9O_{34}]^{9-}$ ligands in **1**. We also note here that $K_{10}Na_3[Pd^{IV}(O)(OH)\text{-}P_2W_{19}O_{69}(OH_2)]$,[85] with one bridging $[(H_2O)W{=}O]^{4+}$ unit between the two $[A\text{-}PW_9O_{34}]^{9-}$ moieties, is more stable in solution than the Pt-oxo complex, $K_7Na_9[Pt^{IV}(O)(OH_2)P_2W_{18}O_{68}]$, with no such bridging units. These collective findings lead us for the first time to use a polytungstate, $[P_2W_{20}(OH_2)_2O_{70}]^{10-}$, **3a** (the polyanion of **3**), as a ligand for late-transition metal-oxo complexes. This monovacant, clam-shell-like polyanion, **3a**, has two $[(H_2O)W{=}O]^{4+}$ units bridging the two $[A\text{-}PW_9O_{34}]^{9-}$ moieties and provides the most hydrolytically stable late-transition metal oxo complexes to date. Reaction of $AuCl_3$ with **3** in water at 55 °C results in a dark red solution, which on cooling, affords red crystals of $K_7H_2[Au(O)(OH_2)P_2W_{20}O_{70}\text{-}(OH_2)_2]\cdot 27H_2O$ (**2**) in 78% yield, a Au-oxo complex that is stable in aqueous solution at autogenous pH and in the absence of reducing agents.

Purity of the Au-Oxo Complexes 1 and 2. Several techniques established the purity of the bulk samples (versus the analyzed single crystals) of both **1** and **2**. First, elemental analysis conducted on all major elements (three separate determinations for the Au content in **1**) confirmed the purity of both compounds. Second, ^{31}P NMR showed only one peak for both **1** (−8.70 ppm) and **2** (−13.15 ppm), a result consistent with the C_{2v} symmetry of these polyanions established by X-ray crystallography (addressed below; Figure 1). The ^{31}P NMR chemical shifts for all the other phosphotungstates, including

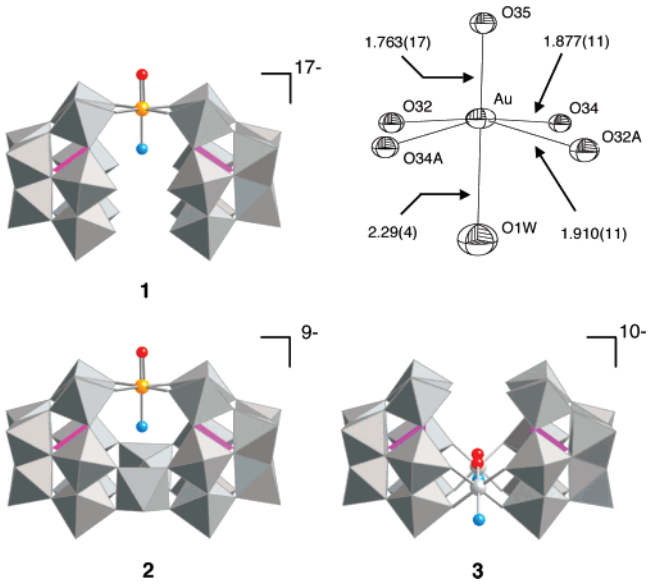

Figure 1. Combination polyhedral/ball-and-stick representations of polyanions **1**, **2**, and $[P_2W_{20}O_{70}(OH_2)_2]^{10-}$ (**3**), the stabilizing ligand of **2**. The WO_6 (or W atom) and PO_4 polyhedra are shown in gray and pink. The Au, O atoms, and aqua (H_2O) ligands are shown in yellow, red, and blue. At the top right is the X-ray structure around the Au atom in **1**. A short Au−O_{oxo} (1.763(17) Å) bond is *trans* to a longer Au−OH_2 (2.29(4) Å) bond, and the central Au atom is displaced out of the equatorial O_4 plane toward the terminal oxo by 0.31(1) Å. The coordination sphere around the Au atom in **2** is almost identical to that in **1** (Au−O_{oxo}, 1.77(4) Å; Au−OH_2, 2.32-(6) Å; doming distance of the Au atom, 0.32(1) Å). The two tungsten units linking the two $[A\text{-}PW_9O_{34}]^{9-}$ units in **3** are shown in ball-and-stick notation. The short, inward-oriented W−O_{oxo} (1.696(13), 1.701(14) Å) bonds in **3** are *trans* to the longer, outward-oriented W−OH_2 (2.265(15), 2.306(14) Å) bonds.

$[P_2W_{19}(OH_2)O_{69}]^{14-}$ (**P_2W_{19}**), $[P_2W_{20}(OH_2)_2O_{69}]^{10-}$, and the reactant $[A\text{-}PW_9O_{34}]^{9-}$ are different. Third, the ^{17}O NMR spectra indicate the samples are pure. The additional evidence revealed by these spectra is addressed below. Fourth, the very-low-temperature optical spectroscopy, cyclic voltammetry, and FT-IR spectra (Figure S1) are also consistent with pure complexes (data elaborated below). Fifth, all the above data are in agreement with the formulations of the two complexes based on the diffraction studies of the isolated single crystals. The only sample impurity in any of the experiments in this article was the very large single crystal analyzed by neutron diffraction. As explained in the neutron diffraction section below, some $[P_2W_{19}O_{69}(OH_2)]^{14-}$ formed during the 3 weeks required for growing the crystal of **1**, and this cocrystallized with **1**. Importantly, the W impurity at the Au position was not only detected in this very large crystal but also quantified from the crystallographic refinement. A ^{31}P NMR spectrum when this large single crystal was dissolved confirmed this impurity and the cocrystallization: the same quantity of all-tungsten compound, $[P_2W_{19}O_{69}(OH_2)]^{14-}$ (33%), and **1** (67%) indicated by the refinement was present.

X-ray Crystal Structures of 1 and 2. Given the improbability of terminal Au-oxo complexes, we established both structural types represented by **1** and **2** using single-crystal X-ray diffraction. The polyhedral/ball-and-stick representations for both are shown in Figure 1 (thermal ellipsoid plots and numbering scheme for **1**, **2**, and **3** are given in Figure 2 and S8). Datasets on three different crystals of **1** were solved at 173 and 96 K, and two of these are summarized in Table 1. Crystallographic studies of crystalline **1** established that it is

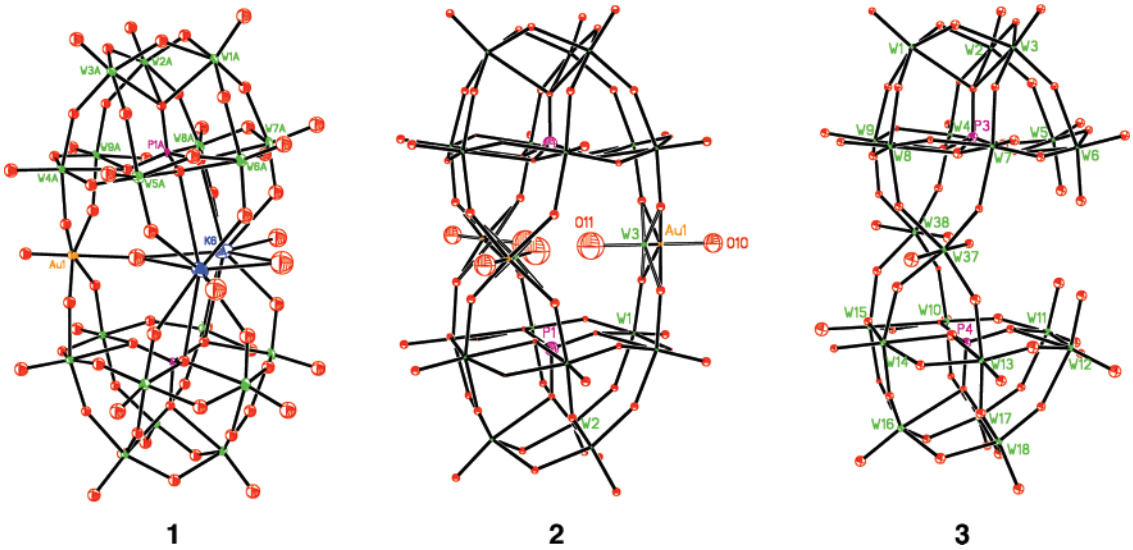

Figure 2. Thermal ellipsoid plots and numbering scheme for **1** (173(2) K), **2**, and **3**.

isostructural to the previous Pt-oxo complex, $K_7Na_9[Pt^{IV}O(OH_2)P_2W_{18}O_{68}]$;[83] the Au−$O_{oxo}$ bond at 1.763(17) Å is the shortest gold−oxygen bond in the literature and clearly in the range of terminal multiply bonded transition metal-oxo species.[1,6] The distance to the ligand *trans* to the terminal oxo is 2.29(4) Å, strongly suggesting a dative (coordination) Au−OH_2 bond. Covalent single Au−O bonds, many of which have been structurally characterized in both gold oxides[69] and recently reported soluble gold complexes with bridging oxo groups[72,73] are shorter (in the range of 1.90−2.10 Å). The Au atom in **1** is coordinated by four other oxygen atoms from two symmetry equivalent polytungstate ligands that define a square O_4 equatorial plane in approximate C_{2v} symmetry. The central Au atom is displaced out of the plane toward the terminal oxo ligand by 0.31(1) Å; this "doming" is a nearly universal feature exhibited by terminal metal-oxo units. Two potassium cations located in the cavity between the two polytungstate units doubtless stabilize the entire sandwich structure by linking the two $[A\text{-}PW_9O_{34}]^{9-}$ frameworks. All three X-ray structure determinations of **1** are disorder-free in the polyanion (**1a**) unit and give the same distances and angles; thus, we take these values to be definitive. In the structure of **1**, the *trans* aqua ligand (oxygen O1W) has large thermal parameters. This results from a slight displacement of this oxygen from the C_2 axis (through the oxo oxygen, Au, and aqua oxygen) by potassium ions and phosphate oxygens O27 that are within the van der Waals distance of O1W.

In contrast to **1**, the polyanion unit of **2**, $[Au(O)(OH_2)P_2W_{20}O_{70}(OH_2)_2]^{9-}$ (**2a**), is disordered. However, this type of disorder (about the C_3 axis resulting in crystallographically imposed D_{3h} symmetry on the C_{2v} molecule) has been noted in the isostructural all-tungsten complex $[P_2W_{21}O_{71}(OH_2)_3]^{6-}$ in which the $(H_2O)Au(O)$ is replaced by $(H_2O)W(O)$,[92] and it can be well modeled. Polyanion **2a** has C_{2v} symmetry and crystallizes in the hexagonal space group $P6_3/mmc$. The site symmetry of the P atoms is 3*m* (C_{3v}), imposing the principal three-fold axis (vertical) on the crystal structure. In addition, all atoms on the equatorial plane (including W, Au, and their terminal oxo and aqua groups) sit on the *mm* symmetry sites; therefore, the anion exhibits a crystallographically imposed D_{3h} symmetry overall. The consequence of this imposed symmetry is an overall apparent disorder in the equatorial plane of the anion. The two W atoms on the equatorial plane, as well as their outward-oriented aqua ligands and inward-oriented oxo groups, are evenly split on the three interior *mm* sites (ideal site-occupancy factor 2/3). On the other hand, the Au atom, along with its external (outward-directed) oxo and inward-directed aqua group, is disordered over the three exterior *mm* sites (ideal site-occupancy factor 1/3). The refined site-occupancy factor is approximately 65:35 for W and Au, respectively, rather than 67:33. This result suggests that a few of the tungsten sites are vacant in the crystal, resulting in a slightly higher weight for Au occupancy. This disorder model (on the initial polytungstate, $[P_2W_{21}O_{71}(OH_2)_3]^{6-}$) was revealed in part by careful ^{183}W NMR work by Tourné and co-workers.[92] One test of the validity of the disorder model is that all the key distances in **2** including Au−O_{oxo}, Au−OH_2 (aqua ligand *trans* to oxo ligand), Au−OW (Au−O bonds in the equatorial plane), and Au−C_t (displacement of Au out of the mean equatorial O_4 plane toward the terminal oxo group) are almost identical within experimental error to those in the triply determined disorder-free structure of **1** (Au−O distances for both compounds are given in the Figure 1 caption), indicating nearly identical $Au(O)(OH_2)(O-W)_4$ coordination spheres in both structures. ^{31}P NMR confirmed the purity of the samples from which the single crystals of **1** and **2** for diffraction were obtained: no phosphotungstates of any kind, including $[P_2W_{21}O_{71}(OH_2)_3]^{6-}$, were present in either sample.

Neutron Diffraction Studies. Although we felt the distances in the Au-oxo units in both **1** and **2** were unequivocal based on the disorder-free X-ray structures of **1**, we endeavored to use two additional methods to assess this unprecedented structure, Au EXAFS and neutron diffraction. As expected, interference from the 18 or 20 tungsten atoms in **1** and **2** made Au EXAFS highly problematical (Table S2),[110] but neutron diffraction was informative.

As an independent structural technique, neutron diffraction can determine not only the absolute structure of molecules but also the location of hydrogens. The latter are effectively never located in even the best X-ray crystallographic structure determinations of polytungstates. As shown in Figure 3A, examinations of the neutron Fourier maps around O35 do not

(110) Bearden, J. A.; Burr, A. F. *Rev. Mod. Phys.* **1967**, *39*, 125−142.

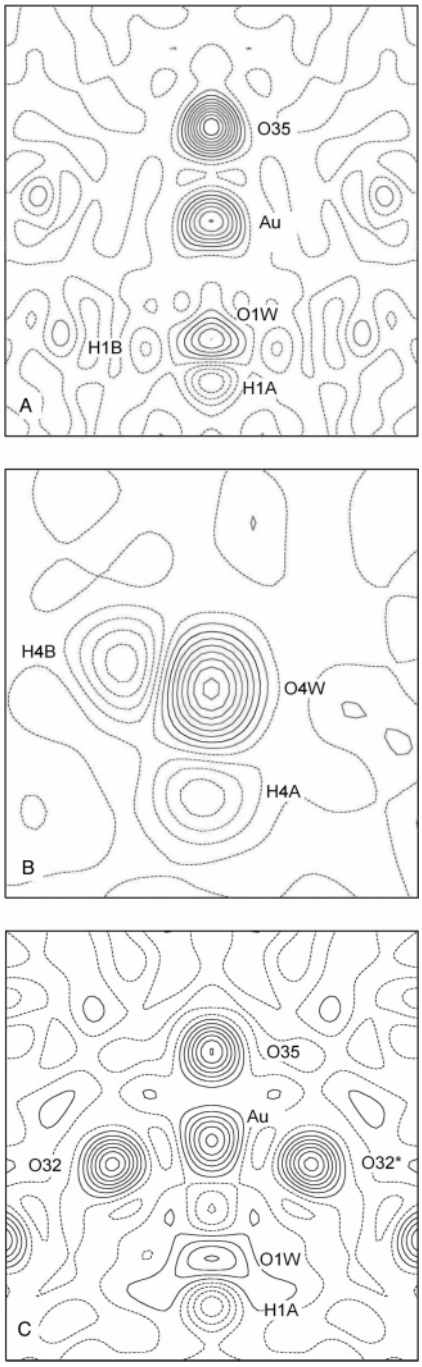

Figure 3. F_{obs} Fourier map sections derived from single-crystal neutron TOF Laue diffraction data taken at 30 K on **1**. Atom positions are labeled. In these sections, all non-hydrogen atoms have positive scattering density (solid contour lines), and hydrogen atoms have negative scattering density (dashed lines). (A) Fourier map section (8 Å on an edge) along the Au-O35−O1W 2-fold symmetry axis and between the equatorial POM ligands bonded to Au, showing negative scattering density near O1W, indicative of a disordered aqua ligand. Because of the disorder, the protons on O1W were not included in the refinement. Low level negative contours located near O35 could not be refined with any reasonable fractional occupancy. (B) Fourier map section (4 Å on an edge) showing a well-modeled water molecule (O4W−H4A−H4B) in the same asymmetric unit as Figure 3A. Note that no such feature indicative of a hydrogen atom is seen close to O35 in Figure 3A. (C) Fourier map section (8 Å on an edge) from the Au-O35−O1W−O32−O32* plane. The crescent-shaped scattering density at O1W indicates disorder of the aqua ligand about the 2-fold axis. This situation leads to an unreasonably short Au−O1W distance (1.98(3) Å). The actual distance is longer (2.29(4) Å). The negative scattering density is attributed to hydrogen, but because of the disorder, atom H1A was not included in the refinement.

show the significant negative scattering density that is seen around water oxygen O1W, thus ruling out the possibility that a hydrogen atom is bound to the oxo ligand. In short, the Au−O_{oxo} distance, the doming, and the lack of a hydrogen on the oxo oxygen are three arguments from diffraction studies alone that these complexes are terminal Au-oxo complexes and not Au-hydroxo complexes. Unlike Au-oxo species, Au-hydroxo complexes, while unusual and rare, are nonetheless precedented.[111,112] The negative density, indicated by dashed contours, observed in the Fourier maps in the area surrounding O1W is attributed to the presence of hydrogen atoms. However, considering the disorder found in this ligand, the hydrogen atoms were not included in the refinement. In Figure 3B, it can be seen that H4A and H4B are clearly localized and bound to O4W. O4W is in the asymmetric unit, and its nearest neighbors are O15 (also in the asymmetric unit) and O4 (related by the $-x + 1/2$, $-y$, $-z + 1/2$ symmetry operator). Besides O4W, there are four additional water oxygen atoms with negative density that successfully model as hydrogen atoms. This section of the map shows the kind of negative scattering density that would lead to a hydrogen atom assignment, and it is clear that no such feature is seen close to O35. Figure 3C presents the Fourier map section from the Au−O35−O1W−O32−O32* plane. The crescent-shaped scattering density at O1W indicates disorder of this aqua ligand about the 2-fold axis. This is consistent with the observation in the X-ray structure of **1** that oxygen O1W has large thermal parameters resulting from slight displacement of this oxygen from the C_2 axis by potassium ions and phosphate oxygens O27 that are within the van der Waals distance of O1W. The negative scattering density is attributed to hydrogen, but because of the disorder, atom H1A was not included in the refinement.

During initial refinements it was noticed that the isotropic displacement parameter for Au was large in comparison to other heavy atoms in the structure. The all-tungsten compound isostructural to the Au-oxo complex **1**, namely $[P_2W_{19}O_{69}(OH_2)]^{14-}$, a hydrolytic decomposition product of **1**, forms during the 3-week process required to grow the giant single crystal required for the neutron diffraction study. Independently, we demonstrated using ^{31}P NMR that **1** (but not **2** which is stable in solution) hydrolyzes to form several tungstates including monomeric tungstate and the polytungstate ligand used in the synthesis initially, $[A\text{-}PW_9O_{34}]^{9-}$, and that the latter and tungstate form $[P_2W_{19}O_{69}(OH_2)]^{14-}$ under the crystallization conditions. Once formed, $[P_2W_{19}O_{69}(OH_2)]^{14-}$ cocrystallizes with **1**. This is not surprising given that these two polyanions are nearly isostructural and have similar charges. Thus, in the very large crystal submitted to neutron diffraction studies, some of the molecules have Au at this position and others have W at this position. The fractional occupancy of the Au site was then freely refined to a value of 0.878. Calculations from this value and the scattering lengths of Au and W reveal that the central metal site is populated with 67% Au and 33% W (detailed calculations are in the Supporting Information). Despite the cocrystallization, the large crystal was of very high quality and the data analysis confirmed the presence of both the Au-oxo unit (no hydrogen proximal to the oxo oxygen) and the aqua ligand *trans* to the oxo position (both aqua hydrogens, despite

(111) Cinellu, M. A.; Minghetti, G.; Pinna, M. V.; Stoccoro, S.; Zucca, A.; Manassero, M. *J. Chem. Soc., Dalton Trans.* **2000**, 1261−1265.
(112) Cinellu, M. A.; Minghetti, G. *Gold Bull.* **2002**, *35* (1), 11−20.

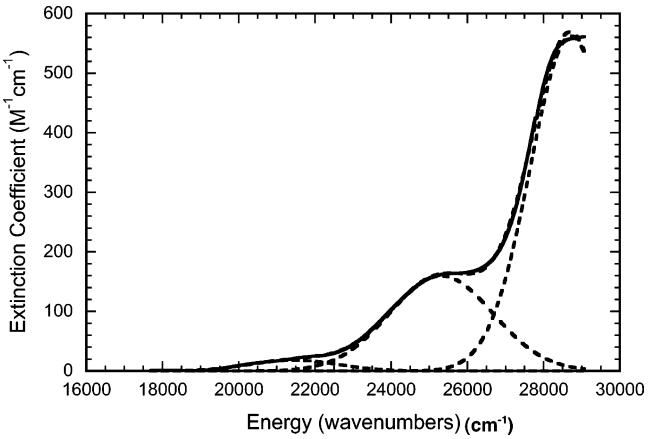

Figure 4. Low temperature (17 K) electronic absorption spectrum of **2** in a 1:3 water−glycerol glass with band deconvolution.

positional disorder, were located; Figure 3). It is worth noting that neutron diffraction is a well-established tool for distinguishing neighboring elements in the periodic table or isotopes of the same element in those cases where the neutron scattering lengths are sufficiently different, including H versus D.[113] In the case of W and Au, with scattering lengths of 4.86 and 7.63 fm, respectively, neutron diffraction data can easily determine the relative occupancies of sites occupied by both elements. Cocrystallization of **1** and $[P_2W_{19}O_{69}(OH_2)]^{14-}$ was confirmed by ^{31}P NMR. Importantly, ^{31}P NMR and other techniques also established that the small crystals of **1** (usually obtained in 1 day) submitted for repeated elemental analysis and used in all the other experiments contained no detectable phosphorus impurities including $[P_2W_{19}O_{69}(OH_2)]^{14-}$.

Optical Spectroscopy. Very-low temperature (17 K) electronic absorption data were collected for **2**, the more stable complex. The sample was dissolved in a 1:3 water:glycerol mixture in order to obtain a good optical glass; the spectrum (Figure 4) possesses two weak absorption bands, at 21 440 cm^{-1} (466 nm, band 1) and 25 310 cm^{-1} (395 nm, band 2), with extinction coefficients of 18 and 160 M^{-1} cm^{-1}, respectively. The Au(III)-to-W(VI) and more intense oxygen-to-W(VI) charge-transfer bands are found at higher energy (E > 26 000 cm^{-1}). Our analysis of the ligand field spectrum of **2** is based on our previous assignments of the unprecedented Pt(IV)-oxo and Pd(IV)-oxo sites bound by POM ligands and assumes a strong ligand field imparted on the metal center by the bridging and terminal oxo ligands. On the basis of our previous studies of high-valent transition metal complexes with a single terminal oxo ligand, we anticipate a similar d orbital splitting pattern with the metal d_{z^2} orbital highest in energy due to strong antibonding interactions between the terminal oxo p_z orbital and the Au d_{z^2} orbital. Similarly, strong π antibonding interactions between the terminal oxo $p_{x,y}$ orbitals and the Au $d_{xz,yz}$ destabilize the latter orbitals. The d_{xy} orbital is higher in energy than the π antibonding $d_{xz,yz}$ orbitals because it is σ antibonding with respect to the four equatorial oxygens (W−O− ligands). For a d^8 system, this yields a diamagnetic ground state with a $(d_{x^2-y^2})^2(d_{xz})^2(d_{yz})^2(d_{xy})^2(d_{z^2})^0$ orbital configuration in C_{2v} symmetry. Using this ground state electronic configuration and ligand field splitting pattern, ligand field transitions occur from the doubly occupied Au based d orbitals to the empty Au d_{z^2} orbital, and we can now make tentative assignments for the observed Au(III) ligand field bands. The lowest energy ligand field one-electron promotion will therefore be $xy \rightarrow z^2$. Since there are no additional transitions found at energies down to 5,000 cm^{-1} in the room temperature solution electronic absorption spectrum we can make tentative assignments for the 21 440 cm^{-1} and 25 310 cm^{-1} ligand field bands as $xy \rightarrow z^2$ ($^1A_1 \rightarrow {}^3A_2$) for band 1 and $xy \rightarrow z^2$ ($^1A_1 \rightarrow {}^1A_2$) for band 2. The $^1A_1 \rightarrow {}^1A_2$ transition is symmetry forbidden in the local C_{2v} symmetry, and its intensity likely derives from a combination of vibronic coupling and small static distortions that lower the symmetry from idealized C_{2v}. The weak spin-forbidden $^1A_1 \rightarrow {}^3A_2$ transition gains intensity by spin−orbit coupling with its spin-allowed $^1A_1 \rightarrow {}^1A_2$ partner. This assignment leads to a $d_{xy}-d_{z^2}$ orbital splitting (e_g splitting) of ∼25 000 cm^{-1} due to the strong terminal oxo ligand field. The equatorial oxo ligand field is likely markedly weaker than the axial field due to the fact that the O_{eq} ligands are bridging to high valent W(VI) centers while the axial oxo is terminal. Finally, the experimentally determined $^1A_2 \rightarrow {}^3A_2$ splitting of ∼4000 cm^{-1} may be compared with an ∼4000 cm^{-1} $^1E \rightarrow {}^3E$ splitting observed in the ligand field spectrum of d^2 $[MoOL_4Cl]^{1+}$ complexes,[114] lending further support for our assignment of the lowest ligand field states for **2** as being composed of exchange split singlet and triplet $xy \rightarrow z^2$ excitations. Despite marked efforts, these orbital and electronic transition assignments could not be confirmed by DFT calculations because the complexes and models thereof are unstable (see computational section below).

pH Dependent UV−vis Titrations of 2. The *trans* ligand to the terminal Au-oxo unit in the polyanion of **2** was further confirmed by pH-dependent UV−vis titrations. The ambient temperature UV−visible spectrum of **2** in aqueous solution does not change when the pH is dropped to as low as 0.38. In contrast, the analogous pH titration of the Pd-oxo complex, $K_{10}Na_3[Pd^{IV}O(OH)P_2W_{19}O_{69}(OH_2)]$, in which the ligand *trans* to the Pd-oxo unit is a hydroxyl group, does induce readily observed (fairly dramatic) changes in the UV−visible spectrum.[85] Also consistent with the presence of a trans aqua ligand in **2** is that the UV−vis spectrum in water changes when titrated with base: changes are clearly apparent at *ca.* pH 5.8 (a red shift and an increase in ϵ, Figure S9), and this change continues until a pH value of *ca.* 7.5 is reached. Moreover, this process is fully reversed by subsequently decreasing the pH by addition of HCl; the *trans* hydroxo ligand is re-protonated to the aqua ligand. Thus acid-based titrations monitored by electronic absorption spectroscopy confirm the finding of the X-ray and neutron diffraction studies that an aqua ligand is *trans* to the Au-oxo unit in **2**.

Electrochemistry. The voltammetric behavior of the Au-oxo complexes set up the controlled potential coulometry experiments that are of central importance in assigning the Au oxidation state of these unique compounds. Since the Au oxidation state is by no means clear from the usual inferences, care was taken to see that all the electrochemical measurements were fully reproducible. Likewise, the chemical (reductive) titrations of the Au-oxo complexes in the next section have considerable importance and were accorded similar consideration. A typical cyclic voltammogram (CV) of 2.0 mM **2** in

(113) Kurihara, K.; Tanaka, I.; Chatake, T.; Adams, M. W. W.; Jenney, Jr., F. E.; Moiseeva, N.; Bau, R.; Niimura, N. *Proc. Natl. Acad. Sci. U.S.A.* **2004**, *101*, 11215−11220.

(114) Re, R. E. D.; Hopkins, M. D. *Inorg. Chem.* **2002**, *41*, 6973−6985.

0.4 M sodium chloroacetate buffer (pH 3) is shown in Figure S5. This CV is somewhat similar to that reported for Pd-containing polytungstates. We assign the first reduction wave at *ca.* 420 mV to a reduction of Au(III) to Au(0), which is deposited as a Au(0) film on the working electrode. The second reversible wave at −590 mV ($\Delta E \sim 60$ mV) is a reduction of tungsten (see below). An additional peak is observed at quite high potential (1100 mV; data not shown). The current intensity of this peak dramatically increases with number of CV runs and is attributed to the oxidation of deposited Au(0) on electrode surface followed by reduction of the oxide. The thickness of Au(0) film increases with number of runs, which results in an increase of the current associated with the peak. At the same time the current intensity of peak at 420 mV decreases with number of CV runs. Similar CVs are observed at lower scan rates, 25 and 2 mV/s (data not shown). A CV of the same buffer solution (no **2** present) obtained using the working electrode with deposited Au(0) (after 11 runs with a scan rate 100 mV/s) shows the same peak at 1100 mV. The current intensity of the peak does not increase with number of runs (no more deposition of Au(0) takes place). The reversible peak at −590 mV is assigned to the reduction of tungsten in **2** (or in $\mathbf{P_2W_{20}}$, the demetalated POM). Indeed, a CV of 0.5 mM $K_{10}[P_2W_{20}(OH_2)_2O_{70}]\cdot 22H_2O$ in 0.4 M sodium chloroacetate buffer (pH 3) shows the peak at the same potential, −590 mV, with the same current intensity.

CVs of 2.85 mM **1** and 2.0 mM **2** in 0.4 M sodium chloroacetate buffer (pH 3) are shown for comparison in Figure S5. The reduction of Au(III) to Au(0) in **1** solution proceeds at much more negative potential, −290 mV, the approximate value expected given the much higher charge on polyanion **1a** (17-) versus **2a** (9-). The reversible wave at approximately −610 mV, assigned to reduction of tungsten, is ∼20 mV more negative than that for the corresponding tungsten reduction in **2**.

Bulk electrolysis (coulometry at controlled potential) was used to determine the oxidation state of Au in both **1** and **2**. The most detailed studies were conducted on **2** given its higher stability in solution relative to **1**. The number of electrons required for complete reduction of **2** was determined over a range of applied reduction potential, concentration of **2**, and buffer solution (sodium chloroacetate). An increase in the concentration of buffer (0.2 or 0.4 M), a decrease in the concentration of **2** (4.2 or 1.0 mM), or application of a more negative potential (350 or 50 mV) results in a formal increase in the number of electrons transferred, *n*, from 3.3 to 4.1 (the latter number may significantly increase with increase of electrolysis time). Under these conditions, the current quickly drops after ∼20 min of electrolysis and then reaches a plateau (a "background" current). A contribution of this "background" current to a total charge was estimated from controlled potential electrolysis carried out in a buffer solution without **2** using an electrode with metal gold deposited on its surface (the electrode from a previous electrolysis of **2**). A second controlled potential electrolysis was carried out using a working electrode after dissolving metal gold in *aqua regia* solution. Both the control (blank) electrolyses produced similar results, while the charge in a second case was ∼20−30% lower. The data were plotted as a dependence of $n = (C - C_b)/\mathrm{FN}$ *versus* time, where *C* and C_b are the numbers of coulombs passed during electrolysis of the Au complex and during blank electrolysis using an electrode with metal gold deposited on its surface. Under minimally optimized conditions (applied potential 350 mV, 0.2 M sodium chloroacetate buffer solution, 4.2 mM **2**), the contribution of C_b to total *C* was less than 15%. A representative curve is given in Figure S6. After such correction for a "background" current, *n* was found to be *ca.* 3.2.

A controlled potential coulometric reduction of **1** was carried out in a similar way to that of **2**. A correction for a background current contribution was done as described in the Experimental Section. The results, given in Figure S6, yield $n = 3.15 \pm 0.2$.

Similar data were collected for bulk electrolysis of $AuCl_3$ and $(NH_4)AuCl_4$. Under optimal conditions (with minimal contribution of a "background" current, in chloroacetate buffer) for $AuCl_3$, *n* was 2.7 ± 0.3, while *n* was 3.0 ± 0.2 for $(NH_4)AuCl_4\cdot 1.3H_2O$ in sulfate buffer in the presence of NaCl (Figure S6). Here it is worth mentioning that $AuCl_3$ is a highly hygroscopic compound resulting in overestimation of molality during weighing. (The molecular weight for $AuCl_3$ was calculated assuming no water was present in the sample.) The amount of coordination water in $(NH_4)AuCl_4\cdot 1.3H_2O$ was determined experimentally using thermogravimetric analysis (TGA).

Chemical Titrations. Reactions of **2** with $ABTS^{2-}$ or $Fe^{II}(CN)_6^{4-}$ are fast and produce the intensively green colored $ABTS^{\bullet-}$ or the yellow $Fe^{III}(CN)_6^{3-}$ during mixing. Both reaction products, $ABTS^{\bullet-}$ and $Fe^{III}(CN)_6^{3-}$, are stable under argon. Their yields were quantified by their characteristic UV−vis spectra. The intensively colored $ABTS^{\bullet-}$ has maxima at 417, 645, and 728 nm, and the $Fe^{III}(CN)_6^{3-}$ has a maximum at 420 nm.

Under typical experimental conditions, addition of 0.02 mM **2** (final concentration) to 2 mM $ABTS^{2-}$ produced 0.04 mM $ABTS^{\bullet-}$. The yield was independent of $[ABTS^{2-}]$ and linearly proportional to the amount of **2** added. On average 2.05 ± 0.15 $ABTS^{\bullet-}$ were formed per equivalent of **2** present. This stoichiometry is consistent with a reduction of Au(III) to a Au(I) species. However, a demetalation of $Au^IP_2W_{20}$ complex to form other stable Au(I) species cannot be ruled out since similar results were obtained in the reaction of $ABTS^{2-}$ with $(NH_4)AuCl_4$. The reduction potential of $ABTS^{\bullet-}/ABTS^{2-}$ is relatively high, 440 mV (SCE), and close to the potential (415 mV) required for electrochemical reduction of **2**. A large excess of $ABTS^{2-}$ over **2** results in complete reduction of Au(III) to Au(I); further reduction of Au(I) to Au(0) is probably unfavorable.

A stoichiometric amount of a stronger reducing agent should completely reduce Au(III) to Au(0). We attempted to use $Fe^{II}(CN)_6^{4-}$ as a reducing agent ($E = 235$ mV vs SCE, determined from CV in 50 mM sodium chloroacetate buffer, pH 3.0, in the presence of 0.3 M KCl). However, the reduction of **2** proceeds to completion only in presence of excess of $Fe^{II}(CN)_6^{4-}$. For example, a mixture of 0.2 mM **2** (final concentration) and an excess of $Fe^{II}(CN)_6^{4-}$ (4.5 mM) produces 2.3−2.6 equiv of $Fe^{III}(CN)_6^{3-}$, consistent with a partial reduction of Au(I) to Au(0). Interestingly, a similar stoichiometry is obtained in the reduction of $(NH_4)AuCl_4$ by $Fe^{II}(CN)_6^{4-}$. Furthermore, if the reaction is carried out in the presence of NaCN (>1 mM), then 2.0 ± 0.1 of $Fe^{III}(CN)_6^{3-}$ are formed per equivalent of **2**. Such a behavior is in agreement with a reduction of Au(III) to Au(I), with the latter stabilized by cyanide anions.

When the stronger one-electron reducing agent, $SiW_{12}O_{40}^{5-}$ ($E = -195$ mV SCE), is used to titrate **2**, Au(0) particles are

quickly produced which preclude quantification of the reaction stoichiometry using UV−visible spectroscopy. Therefore, we monitored the titration of $SiW_{12}O_{40}^{5-}$ by **2** using solution reduction potentials. The potential of the $SiW_{12}O_{40}^{5-}/SiW_{12}O_{40}^{4-}$ solution is controlled by the ratio of reduced and oxidized forms (−230 mV when the ratio is 7). Oxidation of $SiW_{12}O_{40}^{5-}$ by **2** decreases this ratio resulting in a slow increase in reduction potential from −230 mV to −150 mV (corresponding to $[SiW_{12}O_{40}^{5-}]/[SiW_{12}O_{40}^{4-}] = 0.07$). If all $SiW_{12}O_{40}^{5-}$ is oxidized, then the solution reduction potential is controlled by the Au(III)/Au(0) couple. This results in a sharp increase in solution reduction potential (>400 mV, Figure S7). A titration end-point determined from the intersection of two straight lines shown in Figure S7 proves that 3.05 ± 0.15 equiv (average of two independent experiments) of $SiW_{12}O_{40}^{5-}$ are required to reduce 1 equiv of **2**, consistent with the reduction of Au(III) to Au(0). The formation of Au(0) particles is clearly seen. A control titration of $SiW_{12}O_{40}^{5-}$ by $(NH_4)AuCl_4$ gave 3.1 ± 0.15 as the stoichiometric coefficient.

We also attempted to reductively titrate freshly dissolved **1** with three other well-defined and well documented one-electron reductants, $SiW_{12}O_{40}^{5-}$, $AlW_{12}O_{40}^{6-}$, and thiosulfate. Mixing of the blue colored solutions of the one-electron-reduced POMs, $SiW_{12}O_{40}^{5-}$ or $AlW_{12}O_{40}^{6-}$ with a solution of **1** results in an immediate decoloration of solutions; Au(0) particles are formed much more slowly. Addition of **1** to solutions of $SiW_{12}O_{40}^{5-}$ or $AlW_{12}O_{40}^{6-}$ results in a quick increase of solution reduction potential, which then decreases with time. In general, redox titrations with the reagents to well-defined end-points were not highly reproducible. Freshly dissolved **1** does not react with $ABTS^{2-}$ or with $Fe^{II}(CN)_6^{4-}$.

X-ray Absorption Spectroscopy Studies. Complexes **1** and **2** were further studied by X-ray absorption spectroscopy (XAS) to establish the oxidation state of Au. Metal L-edge XAS probes the electronic transition from the metal 2p orbital into the unoccupied molecular orbitals and continuum states. Spin−orbit coupling splits the 2p orbital into the $^2P_{3/2}$ and the $^2P_{1/2}$ states, giving rise to the L_3 and L_2 edges, correspondingly. The L_3 edge possesses the largest edge jump and a smoothly varying background, and thus it is the most widely used L edge to probe the local geometric and electronic structure of a metal atom. Unfortunately as noted above, the high content of tungsten in the Au-oxo complexes, **1** and **2**, despite concerted efforts, precludes the use of the Au L_3 edge for XAS studies of these complexes. Specifically, the Au L_3 edge at 11 919 eV occurs just above the W L_2 edge at 11 544 eV, and thus the signal from gold would superimpose with a highly oscillating background from the EXAFS of 18 or 20 tungsten atoms per one gold atom. We therefore used the Au L_2 edge at 13734 eV to collect the Au XAS data. This edge is situated well above all W L edges and the Au L_3 edge (see Table S2 for the list of the energies of L edges for W and Au)[110] and is not affected by their EXAFS. The Au L_2-edge features, also, can be expected to be similar to well-established L_3-edge features because L_2 and L_3 absorption edges are dominated, respectively, by the similar $2p_{1/2} \rightarrow 5d_{3/2}$ and $2p_{3/2} \rightarrow 5d_{5/2}$, $5d_{3/2}$ dipole-allowed transitions. That is, at the L_2 edge the $5d_{3/2}$ final-state density contributes to the transition strength, while at the L_3 edge both $5d_{5/2}$ and $5d_{3/2}$ final-state densities contribute. However, tungsten still absorbs highly at these energies, making the sample nontransparent to X-rays and resulting in a very low signal-to-noise ratio for the Au signal.

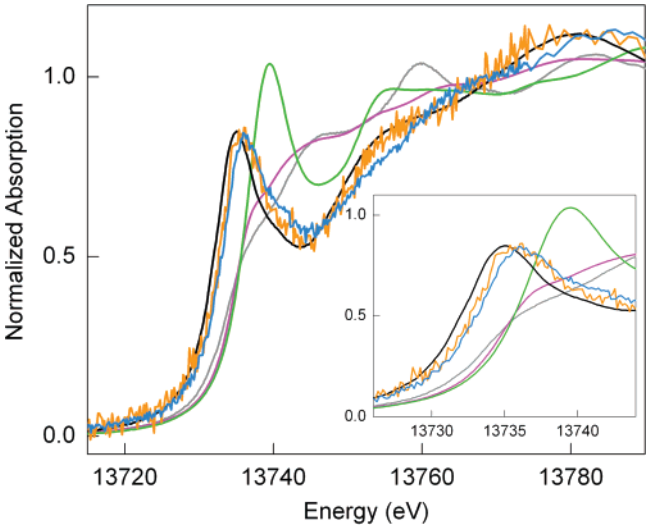

Figure 5. Au L_2 near-edge X-ray absorption spectra of $Au^{III}(CH_3COO)_3$ (black), **1** (orange), **2** (blue), $Na_3Au^I(S_2O_3)_2$ (magenta), $KAu^I(CN)_2$ (green), and Au^0 foil (gray). The edge region is magnified in the inset. Spectra were measured at the Stanford Synchrotron Radiation Laboratory (SSRL) on beam lines 2-3 and 9-3.

The Au L_2-edge XAS spectra of reference compounds $Au^{III}(CH_3COO)_3$, $Na_3Au^I(S_2O_3)_2$, $KAu^I(CN)_2$, and Au^0 foil are shown in Figure 5, with the edge region magnified in the inset. The sharp intense peak observed for Au(III) acetate at the absorption threshold, the so-called "white line", can be attributed to the electronic transitions from the $2p_{1/2}$ level to unoccupied molecular orbitals of $5d_{3/2}$ character, by analogy to a similar feature observed at the Au L_3 edge.[115−118] The intensity and the position of the white line should therefore reflect any variations of the density and nature of the unoccupied *d*-states. This effect is observed for Au(I) sodium thiosulfate and Au foil (Figure 5), for which the white line is nearly absent and it is shifted to higher energy relative to that of Au(III) by 4 eV. Contrary to Au(I) sodium thiosulfate, the spectrum of Au(I) potassium cyanide has an intense white line. This reflects depletion of electron density of the *d*-levels in Au(I) potassium cyanide because of the strong backbonding to the cyanide ligands. The position of the white line in Au(I) potassium cyanide, however, is still indicative of Au(I) as its rising part overlays well with the rising edge of Au(I) sodium thiosulfate. Therefore, the near-edge region at the Au L_2 edge is characteristic of the Au electronic structure and can be used to assign the oxidation state of Au in a sample.

Figure 5 also illustrates the Au L_2 near-edge structure for **1** and **2**. The position and intensity of the white line is very similar in the spectra of **1** and **2** and indicates the same oxidation state for Au in both compounds of interest. The similarity of this feature to the white line of Au(III) acetate suggests, in turn, that Au is present as Au(III) in the polyoxometalate complexes. The comparison of the spectra of **1** and **2** to those of Au(I)

(115) Qi, B.; Perez, I.; Ansari, P. H.; Lu, F.; Croft, M. *Phys. Rev. B* **1987**, *36*, 2972−2975.
(116) Benfield, R. E.; Grandjean, D.; Kroll, M.; Pugin, R.; Sawitowski, T.; Schmid, G. *J. Phys. Chem. B* **2001**, *105*, 1961−1970.
(117) Berrodier, I.; Farges, F.; Benedetti, M.; Winterer, M.; Brown, G. E.; Deveughele, M. *Geochim. Cosmochim. Acta* **2004**, *68*, 3019−3042.
(118) Shaw, C. F.; Schaeffer, N. A.; Elder, R. C.; Eidsness, M. K.; Trooster, J. M.; Calis, G. H. M. *J. Am. Chem. Soc.* **1984**, *106*, 3511−3521.

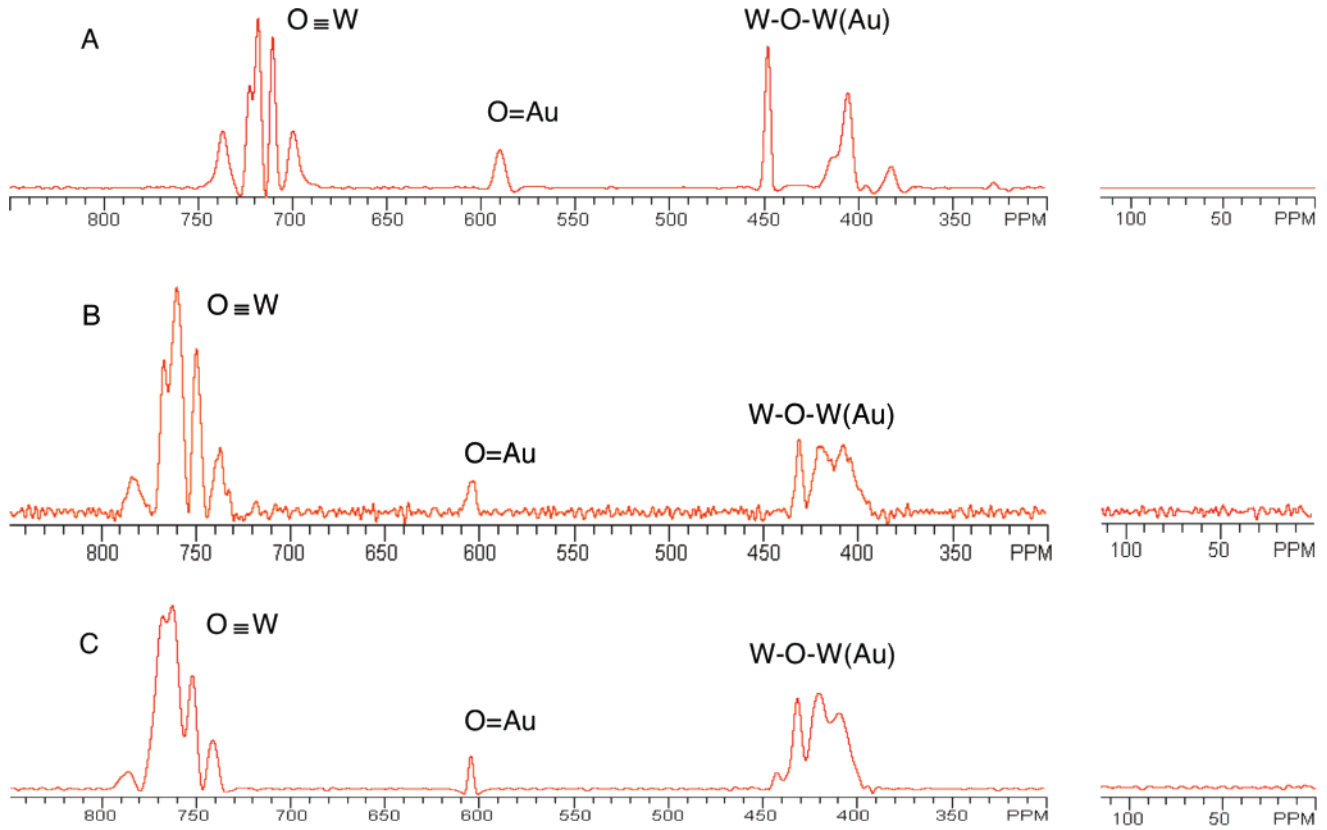

Figure 6. ^{17}O NMR spectra of Au-oxo complexes in 50:50 (v:v) CH_3CN:$CDCl_3$. (A) Tetra-*n*-butylammonium (TBA) salt of **1a**. (B) K⊂*cis*-dicyclohexano-18-crown-6 salt of **2a** enriched in aqueous solution. (C) K⊂*cis*-dicyclohexano-18-crown-6 salt of **2a** enriched in acetonitrile.

compounds provides further evidence of the Au(III) oxidation state in gold-containing polyoxometalates, as the rising part of the edges of **1** and **2** is much closer in energy to Au(III) acetate than to any of the Au(I) complexes. The similarity of the spectra of **1** and **2** suggests a high degree of similarity in the electronic and geometric environment of Au in the two complexes.

^{17}O NMR Experiments. In order to obtain ^{17}O NMR spectra of **1** and **2** in nonaqueous solution, organic soluble forms of both Au-oxo polytungstates are required. The preparation of these, the tetrabutylammonium (TBA) salt of **1a** (TBA**1**) and the K⊂*cis*-dicyclohexano-18-crown-6 salt of **2a**, their isotopic enrichment with ^{17}O, and ^{31}P NMR confirmation of the purity of these enriched Au-oxo complexes are described in the Experimental Section. The ^{17}O NMR spectra for **1** and **2** are shown in Figure 6. The ^{17}O chemical shifts agree well with the general correlation between downfield chemical shift and oxygen π-bond order, a correlation that has been established from both experimental and theoretical studies.[119−124] In the structure of **1**, there are six types of symmetry-equivalent terminal oxo oxygens each residing in a MO_6 coordination unit of approximate local C_{4v} symmetry: five W−O_{oxo} oxygens with an overall triple bond that appear as five peaks well downfield (690−750 ppm), and an Au−O_{oxo} oxygen appearing at 590 ppm. The chemical shifts for oxygen with single covalent bonds to metal centers in metal oxide ligand environments (metal oxides or polyoxometalates) are usually in the range of 250−450 ppm; those for nearly all bridging oxygens in POMs, including **1**, are in the range of 380 to 450 ppm, and that for water oxygen which has effectively no π bonding is *ca.* 0 ppm. The chemical shift for the terminal Au-oxo oxygen is clearly in the range associated with some π bonding although less than for the d^0 W−O_{oxo} units. Since the variable temperature magnetic and NMR data establish that the Au centers in **1** and **2** are absolutely diamagnetic (no low-lying paramagnetic states) and the basic electronic structure (the energies and orientations of the bonding orbitals in the metal-oxo unit) are very similar to those in the d^0 W$(O)_5$−O_{oxo} units, it is reasonable that the π bonding arguments and observed chemical shifts for myriad POMs would apply reasonably well to the terminal oxo oxygen in the Au-$(O)_5$−O_{oxo} units in **1** and **2**. The two ^{17}O NMR spectra of **2** obtained by both aqueous and organic medium enriching methods are similar except that the second spectrum (Figure 6C) for enrichment conducted in an organic solvent has a better signal-to-noise ratio than the first one (Figure 6B). In the structure of **2**, there are seven classes of symmetry-equivalent terminal oxo positions: six W−O_{oxo} oxygens that appear as five peaks from 730 to 790 ppm and the Au−O_{oxo} oxygen that appears at 605 ppm, an ensemble of chemical shifts that are in good agreement with those in **1**. Similarly, the chemical shifts of the bridging oxygens in **2** are in the range of 400 to 450 ppm.

Stoichiometric Oxo Transfer from 2 to Ph_3P. Addition of triphenylphosphine (Ph_3P) to the K⊂*cis*-dicyclohexano-18-crown-6 salt of **2a** in CH_3CN/$CDCl_3$ under argon immediately

(119) Filowitz, M.; Klemperer, W. G.; Messerle, L.; Shum, W. *J. Am. Chem. Soc.* **1976**, *98*, 2345−2346.
(120) Filowitz, M.; Ho, R. K. C.; Klemperer, W. G.; Shum, W. *Inorg. Chem.* **1979**, *18*, 93−103.
(121) Maksimovskaya, R. I.; Fedotov, M. A. *Zh. Strukt. Khim.* **1981**, *22*, 160−162.
(122) Kintzinger, J. *NMR. Basic Principles & Progress* **1981**, *17*, 1−64.
(123) *^{17}O NMR Spectroscopy in Organic Chemistry*; Boykin, D. W., Ed.; CRC Press, Inc.: Boca Raton, 1991.
(124) Kazansky, L. P.; Chaquin, P.; Fournier, M.; Hervé, G. *Polyhedron* **1998**, *17*, 4353−4364.

Scheme 1

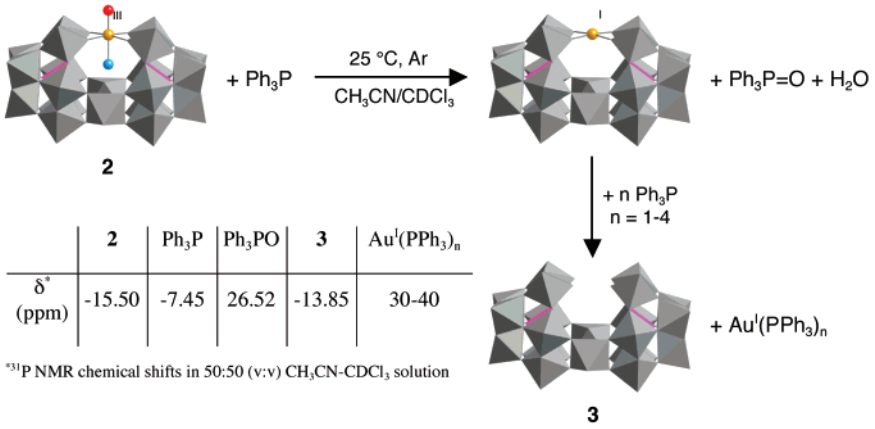

	2	Ph_3P	Ph_3PO	3	$Au^I(PPh_3)_n$
δ^* (ppm)	-15.50	-7.45	26.52	-13.85	30-40

*^{31}P NMR chemical shifts in 50:50 (v:v) CH_3CN-$CDCl_3$ solution

$$[Au^{III}(O)(OH_2)P_2W_{20}O_{70}(OH_2)_2]^{9-} + (n+1)\ Ph_3P \rightarrow [P_2W_{20}O_{70}(OH_2)_2]^{10-} + Ph_3PO + Au^I(PPh_3)_n + H_2O \quad (1)$$

$$[Au^{III}Cl_4]^- + 2\ Ph_3P \rightarrow [Au^I(PPh_3)Cl] + Ph_3PCl_2 + Cl^- \quad (2)$$

yields a clear, colorless solution, and triphenylphosphine oxide (Ph_3P═O, confirmed by ^{31}P NMR spectroscopy). The transformation of the solution from yellow to colorless upon addition of Ph_3P indicates that the terminal oxo on Au is transferred and the Au(III) is reduced to Au(I). This oxo transfer reaction was carefully investigated by both ^{31}P and ^{17}O NMR spectroscopy (Figure S10). In the ^{17}O NMR spectra, the Au═O peak at 605 ppm disappears with the addition of 3 equiv of Ph_3P, and a new peak at 45 ppm, assigned to the oxygen of Ph_3P═O,[125] appears synchronously. Addition of 5 equiv of Ph_3P does not cause a distinct change in the ^{17}O NMR spectra except that the Ph_3P═O peak at 45 ppm increases in size. Production of Ph_3P═O is also confirmed by ^{31}P NMR spectroscopy: a single peak at 26.52 ppm. In addition to the oxo transfer process, ^{31}P NMR spectroscopy establishes that the resulting Au(I) is subsequently demetalated by free Ph_3P molecules, leading to the monovacant polytungstate ligand, $[P_2W_{20}O_{70}(OH_2)_2]^{10-}$, and Au−$PPh_3$ coordination complexes. Exchange of free and Au(I)-bound Ph_3P is more rapid than the ^{31}P NMR time scale and gives rise to peaks for the Au−PPh_3 coordination complexes whose chemical shifts (30−40 ppm)[126] vary with the ratio of Ph_3P to initial **2**. No free Ph_3P peak appears when even 5 equiv of Ph_3P are added to the solution of **2** in $CH_3CN/CDCl_3$. Based on the ^{31}P and ^{17}O NMR results, an oxo transfer reaction followed by a demetalation of Au(I) is illustrated in Scheme 1 (balanced reaction in eq 1). Control experiments involving addition of Ph_3P to a solution of $Au^I(Ph_3P)Br$ (Alfa Aesar) in $CH_3CN/CDCl_3$ give the same behavior as in the presence of **2** (no free Ph_3P peak was detected), and independently, Ph_3P and $\mathbf{P_2W_{21}}$, an all-tungsten compound isostructural to **2**, were shown to give no reaction. In addition, ^{31}P NMR indicates that reaction of $(NH_4)AuCl_4 + Ph_3P$ under identical conditions to the reactions of **2** (same solvent and temperature under an argon atmosphere) produces Ph_3PCl_2 but no Ph_3P═O (detectable limit <1%). The reactions of Au(III) with Ph_3P are well established in the literature (eq 2).[127] In conclusion, these experiments suggest two lines of evidence that the terminal oxo oxygen on the Au center of **2** transfers to an oxo acceptor, Ph_3P. First, the reaction of **2** + Ph_3P leads to Ph_3P═O and Au(I) complex, while the all-tungsten complex isostructural to **2** does not react with Ph_3P under the same conditions. Second, although regular Au(III) complexes oxidize Ph_3P, the oxidized product is not Ph_3P═O but Ph_3PX_2 (X = Cl or Br).

Computational Studies. B3LYP/SDD calculations were conducted on O═$Au(OH_2)(OH)_4^{n-}$, O═$Au(W_2O_9H_4)_2^{n-}$, and O═$Au(OH_2)(W_2O_9H_4)_2^{n-}$, where n = 1 and 3 (with Au(V) and Au(III) centers, respectively) to model the ligand environment of Au in **1** and **2**. However, these calculations were inconclusive because the ligand environment of the Au centers was unstable which indicates that these models are not yet sufficiently close to the actual polytungstate ligands in **1** and **2**. From these studies one concludes that use of the full systems, $K_{15}H_2[Au(O)(OH_2)P_2W_{18}O_{68}]$ and $K_7H_2[Au(O)(OH_2)P_2W_{20}O_{70}(OH_2)_2]$, is necessary to computationally determine the electronic structures and oxidation state of the Au centers. Unfortunately, density functional calculations of such large systems are not technically feasible at present. We have conducted high level (CASSCF and MRSD-CI) computational studies of the diatomic units, AuO, AuO^+, AuO^{2+}, AuO^{3+}, and of $(NC)AuO^{q+}$ (q = 0, 1, and 2). The findings (electronic structures and oxo dissociation energies) of these studies, summarized in the Supporting Information, while certainly of interest, are not highly insightful regarding the properties of **1** and **2** because the latter Au-oxo compounds are far more complicated and quite likely distinct electronically in multiple ways from these simple diatomic and tetra-atomic units. Comparisons of these calculated results with the experimental data indicate that the Au-oxo units in **1** and **2** have multiple bond character similar to $(AuC)^+$ and related species calculated by Pyykkö and co-workers.[128,129]

Discussion

Syntheses. Formation of the Au-oxo complexes requires the use of particular Au precursor complexes ($AuCl_3$ is best), pH, and ionic strength. The best pH values are those in which the polytungstate ligands are stable. Complex **1** is not stable in aqueous solution but it is stable in organic solvents (e.g., CH_3-

(125) Evans, Jr., S. A. In *^{17}O NMR Spectroscopy in Organic Chemistry*; Boykin, D. W., Ed.; CRC Press: Boca Raton, FL, 1991; Vol. 10, pp 303−308.
(126) Parish, R. V.; Rush, J. D. *Chem. Phys. Lett.* **1979**, *63*, 37−39.
(127) Laguna, A. In *Gold: Progress in Chemistry, Biochemistry and Technology*; Schmidbaur, H., Ed.; John Wiley & Sons: Chichester, UK, 1999; pp 350−427.
(128) Barysz, M.; Pyykkö, P. *Chem. Phys. Lett.* **1998**, *285*, 398−403.
(129) Pyykkö, P.; Riedel, S.; Patzschke, M. *Chem. Eur. J.* **2005**, *11*, 3511−3520.

CN and $CHCl_3$ solutions). Au-oxo complexes **1** and **2** are best rendered soluble in organic solvents by metathesis with TBA cation or by addition of K^+-specific crown ethers, respectively. Bromide, either as the reactant $AuBr_3$ or as a metathesis precursor, TBABr, must be avoided because it reduces the Au-oxo centers.

Atomic Occupancy at the Au Position. The skeptical reader might require specific evidence that Au and Au only resides at this position in the structures and not W or a mixture of W and Au (and that the one Au atom established from the multiple full elemental analyses is not distributed over the polyanion units, **1a** and **2a**). All the diffraction work unequivocally rules out cationic Au counterions to polyanions **1a** and **2a**. There are at least seven arguments that we feel collectively provide compelling evidence for the Au atom residing only at the one central bridging position indicated in X-ray structures of **1a** and **2a**. First, the ^{31}P NMR spectra would show multiple peaks if the Au atom resided at a second (or additional) position(s), but only one singlet is seen for both complexes (chemical shift values in D_2O and organic solvents are given above). In addition, the ^{31}P NMR spectrum indicates that **2** is stable in aqueous solution in the presence of other polytungstates, including $\mathbf{P_2W_{21}}$ which is isostructural to **2** (if the Au were to be replaced by W). This finding, in turn, shows that the polyanions do not undergo metal exchange or any other kind of isomerization in solution. Second, the ^{17}O NMR spectra show a single peak for the Au-oxo oxygen with the expected chemical shift. In addition, the other peaks in the spectra are correct for the polyanion structures indicated by the X-ray structures. Third, the displacement of the Au and W atoms in the metal-oxo units out of the equatorial plane (the doming distance) is 0.31 Å and 0.45 Å, respectively, a difference that is well outside the experimental error in the X-ray structures. All the W-oxo units in both **1a** and **2a** average near 0.45 Å. Fourth, the terminal Au-oxo distances in **1a** and **2a** (both 1.77 Å) are both longer than all the terminal W-oxo distances (1.67 Å) in each structure, and the difference in these distances is outside experimental error. Fifth, the redox titrations and sixth the coulometry are consistent with a single type of Au center in both complexes. Seventh, the one and only sample that does have some W at the Au position, namely the very large single crystal used in the neutron diffraction, does contain both W and Au at this position (a cocrystallization of **1** and the isostructural all-tungsten compound, $\mathbf{P_2W_{19}}$). Not only can this Au/W mixture be quantified (67% Au and 33% W) from the final refined neutron diffraction data, but this same ratio can also be confirmed when this crystal is dissolved and the ^{31}P NMR spectrum obtained. On consideration of all these points, the only possibility is that the single Au atom per polyanion resides at the bridging central position indicated by the X-ray structures.

Au Oxidation State. Five independent techniques are consistent with Au(III) d^8 electronic configurations in **1** and **2**: (a) chemical titrations on both complexes indicate that 3 electrons per polyanion are required to produce Au(0); (b) coulometric measurements also indicate that three electrons convert the Au-oxo complexes to Au(0) (indeed, bright Au mirrors are produced in the bulk electrolysis experiments); (c) the optical spectrum of **2** in water−glycerol glasses at 17 K is distinct from the optical spectrum of the d^6 Pd(IV)-oxo complex and consistent with a d^8 electronic configuration in a six-coordinate C_{2v} structure that is clearly present in **1** and **2** from all the diffraction studies (both **1a** and **2a** exhibit approximate local C_{4v} symmetry around the Au atom in the $Au(O)(OH_2)(O-W)_4$ primary coordination sphere); (d) the Au L_2 near-edge X-ray absorption spectra of both **1** and **2** are consistent with Au(III) centers in both complexes; (e) a careful comparison of the X-ray crystal structures of the isostructural Pt(IV)-oxo complex and **1**. This comparison reveals a fifth strong argument for the d^8 Au(III) electronic configuration in the latter. Both the Pt-oxo[83] complex and **1** are isostructural, have similar cations, and were crystallized out of unbuffered aqueous solution, and therefore detailed comparison of the two structures is defensible. As expected, the M(Pt or Au)-oxo oxygen distances are quite different (1.720(18) and 1.763(17) Å for Pt and Au, respectively). The increased length by 0.043 Å for the Au-oxo unit is well outside experimental error and is consistent with additional electrons populating d-based orbitals on the Au center. A qualification on this point, however, is that there may be a greater ionic contribution to the Pt(IV)-oxo bond than the effectively isostructural Au(III)-oxo bond. Electron paramagnetic resonance and magnetic circular dichroism spectroscopies are not applicable because both **1** and **2** are diamagnetic.

While these five lines of evidence, collectively, would seemingly provide fairly compelling evidence that **1** and **2** contain Au(III) d^8 centers, we are not yet prepared to absolutely rule out Au(V) d^6 centers. Perhaps the most definitive technique to probe the Au oxidation state would be ^{197}Au Mössbauer spectroscopy because the isomer shift correlates very well with oxidation date (at least in the case of ^{57}Fe Mössbauer spectroscopy[59] and quite likely in the case of ^{197}Au Mössbauer spectroscopy), but strong nonresonance absorption by the many tungsten atoms present rendered the Au signal unobservable for both complexes.

Conclusions

(1) Two terminal Au-oxo compounds, **1** and **2**, have been prepared and characterized by more than 10 physicochemical methods. Appropriate polytungstate ligands stabilize these elusive species sufficiently that they can be isolated and studied. The collective experimental data provide seven arguments given in the Discussion that the single Au atom in both **1** and **2** resides only at the central position indicated by the X-ray structures and not in other positions.

(2) The purity of both **1** and **2** were established by multiple elemental analyses on all elements, ^{17}O NMR, ^{31}P NMR, and indirectly by several additional techniques including cyclic voltammetry, chemical titrations, thermogravimetric analysis, differential scanning calorimetry, and other methods.

(3) Both structural types of terminal Au-oxo compounds represented by **1** and **2** have been established using single-crystal X-ray diffraction and exhibit nearly identical $Au(O)(OH_2)(O-W)_4$ coordination spheres with very short $Au-O_{oxo}$ bond distances (1.763(17) for **1** and 1.77(4) Å for **2**). The disorder-free structure of **1** was further corroborated by neutron diffraction studies at 30 K, which also confirmed both the Au-oxo unit (no hydrogen proximal to the oxygen) and the aqua ligand *trans* to the oxo position (both aqua hydrogens, despite positional disorder, were located). The ^{17}O NMR chemical shifts of the terminal oxo groups on Au in both **1** and **2** were also consistent with multiple bonding (and π bonding) between the Au and terminal oxo oxygen.

(4) The results from five independent techniques addressed in the Discussion are consistent with Au(III) d^8 electronic configurations in **1** and **2**. While all these results collectively provide a strong argument for this electronic assignment, we are not prepared to absolutely rule out Au(V) d^6 electronic configurations for these complexes at this time.

(5) Complexes **1** and **2** are well-defined compounds that model the metal oxide-Au interface, exhibit high valent Au centers in metal oxide molecular environments, and reveal more of the fundamental chemistry of gold and oxygen. The structure, reactivity, and other properties of these complexes will be addressed in subsequent studies.

Acknowledgment. We thank NSF (grant CHE-0541752 to C.L.H.), DOE (grant to C.L.H., D.G.M., and K.M.), and NIH (grant GM-057378 to M.L.K.) for support and B. Botar for discussions. The work at Argonne National Laboratory was supported by the DOE Office of Basic Energy Sciences (contract DE-AC-02-06CH11357). X-ray absorption spectroscopy experiments were carried out at the Stanford Synchrotron Radiation Laboratory, a national user facility operated by Stanford University on behalf of the U.S. Department of Energy, Office of Basic Energy Sciences. The SSRL Structural Molecular Biology Program is supported by the Department of Energy, Office of Biological and Environmental Research, and by the National Institutes of Health, National Center for Research Resources, Biomedical Technology Program.

Supporting Information Available: Complete details of the X-ray crystallographic studies and neutron diffraction studies, including five CIF files: complex **1** (both at 173(2) K and 96-(2) K), **2**, **3**, and neutron data on **1**; complete details of magnetism studies, electrochemistry (cyclic voltammetry, controlled potential coulometry), chemical titrations, and ^{197}Au Mössbauer spectroscopy; complete computational studies; Figures S1−S11; Tables S1 and S2; complete ref 108. This material is available free of charge via the Internet at http://pubs.acs.org.

JA072456N